A genetic variant of the Wnt receptor LRP6 accelerates synapse degeneration during ageing and in Alzheimer's disease.

Authors

Megan E. Jones[1, †], Johanna Büchler[1, †], Tom Dufor[1], Ernest Palomer[1], Samuel Teo[1], Nuria Martin-Flores[1], Katharina Boroviak[2], Emmanouil Metzakopian[3], Alasdair Gibb[4], Patricia C. Salinas[1, *]

Affiliations

[1] Department of Cell and Developmental Biology, University College London, London, WC1E 6BT, UK

[2] Wellcome Trust Sanger Institute, Wellcome Genome Campus, Hinxton, Cambridge, CB10 1SA, UK

[3] UK Dementia Research Institute, Department of Clinical Neuroscience, University of Cambridge, Cambridge, CB2 0AH, UK

[4] Department of Neuroscience, Physiology and Pharmacology, University College London, London, WC1E 6BT, UK.

† These authors contributed equally to this work

* Corresponding author. Correspondence: Professor Patricia C. Salinas, p.salinas@ucl.ac.uk

Abstract

Synapse loss strongly correlates with cognitive decline in Alzheimer's Disease (AD), but the underlying mechanisms are poorly understood. Deficient Wnt signalling contributes to synapse dysfunction and loss in AD. Consistently, a variant of the *LRP6* receptor, (*LRP6-Val*), with reduced Wnt signalling, is linked to late onset AD. However, the impact of *LRP6-Val* on the healthy and AD brain has not been examined. Knock-in mice, generated by gene editing, carrying this *Lrp6* variant develop normally. Neurons from *Lrp6-val* mice do not respond to Wnt7a, a ligand that promotes synaptic assembly through Frizzled-5 receptor. Wnt7a stimulates the formation of the LRP6-Fz5 complex but not if LRP6-Val is present. *Lrp6-val* mice exhibit structural and functional synaptic defects that become pronounced with age. *Lrp6-val* mice present exacerbated synapse loss around plaques when crossed to *NL-G-F* AD model. Our findings uncover a novel role for the *Lrp6-val* variant in synapse vulnerability during ageing and AD.

Introduction

In Alzheimer's Disease (AD), memory impairment strongly correlates with synapse degeneration (*1–3*). Synaptic changes occur early in the disease, before amyloid-β (Aβ) plaque formation and neuronal loss (*3*, *4*). At later stages of the disease, further synapse loss is observed around Aβ plaques (*5–8*). It is well documented that the accumulation of oligomeric forms of Aβ triggers synapse dysfunction and degeneration (*3*, *4*, *9*). Numerous studies demonstrate that Aβ oligomers interfere with signalling pathways, which are critical for maintaining synapse integrity, resulting in synapse weakening and loss (*10*, *11*). However, the molecular mechanisms that lead to synapse dysfunction and loss in AD remain poorly understood.

The canonical Wnt signalling pathway, required for synapse function and stability, is impaired in AD (**Figure 1A**) (*12–14*). Wnt ligands and their receptors are expressed in many brain areas affected in AD (https://mouse.brain-map.org/). For instance, many Wnt ligands and Frizzled (Fz) receptors including Wnt7a, Wnt7b, and Frizzled-5 (Fz5), and the Wnt co-receptor LRP6 are expressed in the postnatal and adult hippocampus (*13*,

15–18). However, it is unclear if these ligands and receptors act in an autocrine or paracrine fashion to promote synapse maintenance. Wnt ligands, their receptors and co-receptors play a critical role in synaptogenesis during postnatal development (*18–21*), and in synapse integrity in the adult brain (*12*, *13*, *22*, *23*). The first piece of evidence that Wnt signalling is compromised in AD came from the finding that Dickkopf-1 (Dkk1), a secreted Wnt antagonist, is elevated in the brains of AD patients and in AD mouse models (*24*, *25*). Notably, Dkk1 is required for Aβ-induced synapse degeneration as blockade of Dkk1 protects against Aβ-mediated synapse loss (*14*, *26*). Consistently, *in vivo* expression of Dkk1 in the adult brain induces synapse loss, LTP defects (*12*) and memory impairment (*12*, *27*), as observed in AD mouse models. Second, conditional knockout (cKO) of *Lrp6* in an AD mouse model increases amyloid pathology and exacerbates cognitive deficits (*13*). Third, a genetic link between deficient Wnt signalling and AD came from the identification of three genetic variants of *LRP6* associated with late onset AD (LOAD) (*28*, *29*). Notably, a nonsynonymous SNP (rs2302685) (**Figure 1B**), which has an allele frequency of 0.17 in the European population (*30*), results in a conservative substitution of isoleucine to valine at amino acid 1062 ($LRP6^{Ile\text{-}1062\text{-}Val}$; *LRP6-Val* herein). This substitution is located in the fourth β-propeller of the extracellular domain of LRP6 to which some Wnt ligands bind (*31–33*) (**Figure 1B**). The *LRP6-Val* variant reduces Wnt signalling in cell lines in response to a Wnt ligand (*28*). However, the impact of this variant on brain development, neuronal connectivity and amyloid pathology remains unexplored.

Here, we investigated the impact of the *Lrp6-val* variant on the adult and ageing hippocampus and in the pathogenesis of AD by generating a novel knock-in mouse model using CRISPR/Cas9 genome editing. Homozygous *Lrp6-val* mice developed normally but showed structural and functional synaptic defects in the hippocampus that became more pronounced with age. In these mice, we observed decreased levels of canonical Wnt signalling with age. Notably, neurons from *Lrp6-val* mice were unable to respond to Wnt7a or Wnt3a to promote synapse formation. As Wnt ligands promote the interaction between LRP6 and Fz (*34*), we examined if the LRP6-Val variant affects this interaction by focusing on Fz5, a Wnt7a receptor required for presynaptic assembly in hippocampal neurons (*15*). We found that Wnt7a increased the association between wildtype LRP6 and Fz5, whereas this interaction was significantly impaired in the presence of LRP6-Val.

Consistently, expression of LRP6-Val reduced Wnt signalling. Next, we examined the contribution of the *Lrp6-val* variant to AD pathogenesis by crossing these mice to *hAPP*$^{NL\text{-}G\text{-}F/NL\text{-}G\text{-}F}$ (*NL-G-F)*, a knock-in AD mouse model. The *Lrp6-val* variant significantly increased synapse degeneration in *NL-G-F* mice. Our results demonstrate, for the first time, that the valine substitution in the extracellular domain of LRP6 impairs its Wnt7a-mediated interaction with Fz5, affecting downstream signalling. These findings represent a significant advancement in the Wnt and AD fields by linking a genetic variant that affects Wnt signalling with the pathogenesis of the disease.

Results

LRP6-Val fails to stimulate synaptic assembly and induces spine loss

LRP6 is required for synapse formation and maintenance (*13*, *20*). Furthermore, the *LRP6-Val* variant is linked to late onset AD (LOAD) (*28*), but its impact on neuronal connectivity has not been explored. To assess the effect of LRP6-Val on synapses, we expressed human wildtype *LRP6* (WT *LRP6*) or human *LRP6-Val* in cultured hippocampal neurons. Expression of WT *LRP6* increased the puncta number of vGlut1, a presynaptic marker, along axons (**Figures 1C and 1D**). In contrast, *LRP6-Val* failed to increase the number of presynaptic sites above control cells (**Figures 1C and 1D**). Thus, expression of the *LRP6-Val* variant is unable to induce presynaptic assembly in neurons.

We next examined if the presynaptic assembly induced by expression of WT *LRP6* was ligand dependent as the function of this Wnt co-receptor requires Wnts for signalling (*35*). To block the synaptogenic activity on Wnts in hippocampal neurons, we used the secreted frizzled related protein 1 (sFRP1) (*19*). Addition of sFRP1 blocked the increase in the puncta number of Bassoon, a presynaptic marker, along axons induced by expression of WT *LRP6* **(Figure S1**). However, sFRP1 did not affect the phenotype of cells expressing the *LRP6-Val* variant (**Figure S1**). These results suggest endogenous Wnts are required for LRP6-mediated presynaptic assembly.

We also examined the impact of LRP6-Val on dendritic spines (**Figure 1E**). Expression of WT *LRP6* increased spine head width but had no effect on spine density (**Figures 1E**

and 1F). In contrast, expression of *LRP6-Val* failed to increase spine head width and decreased spine density when compared to control and WT *LRP6* expressing cells (**Figures 1E and 1F**). Thus, *LRP6-Val* is unable to promote dendritic spine growth, whilst inducing spine loss. No differences in puncta number or volume of Homer1, a postsynaptic marker, were found between control and WT *LRP6* expressing neurons (**Figures 1E and 1G**). In contrast, consistent with the reduced number of spines, fewer Homer1 puncta and a decrease in puncta volume were observed in *LRP6-Val* expressing neurons compared to control neurons (**Figures 1E and 1G**). Thus, expression of *LRP6-Val* in neurons decreases the formation of both pre- and post-synaptic sites compared to WT *LRP6*.

Lrp6-val **knock-in mice develop normally and LRP6-Val does not affect its synaptic localisation**

To investigate the *in vivo* role of the *Lrp6-val* variant, we generated a novel knock-in mouse model using CRISPR/Cas9 genome editing. The *Lrp6* A→G point mutation, which results in the substitution of isoleucine for valine, was introduced at the endogenous *Lrp6* locus in the mouse genome, creating a mouse line that carries the *Lrp6-val* variant globally. DNA sequencing confirmed the successful generation of both heterozygous (*Lrp6-val* het) and homozygous (*Lrp6-val* hom) knock-in animals (**Figure 2A**). *Lrp6-val* hom mice developed normally with no visible morphological abnormalities or changes in weight (**Figures S2A and S2B**). Furthermore, *Lrp6-val* het and *Lrp6-val* hom mice exhibited similar synaptic phenotypes (see below). Herein, we primarily focused our attention on *Lrp6-val* hom (*Lrp6-val*) mice.

We next investigated whether the *Lrp6-val* variant was differentially expressed or affected its synaptic localisation. The mRNA and protein levels of LRP6 in the hippocampus of *Lrp6-val* mice were unchanged (**Figures S2C-S2E**). To assess its synaptic localisation, we used structured-illumination microscopy (SIM). Both WT LRP6 and LRP6-Val were present at approximately 80% of excitatory synapses (**Figures S2F and S2G**) but no differences in LRP6 localisation were observed between neurons from WT and *Lrp6-val*

mice (**Figure S2G**). Thus, carrying the *Lrp6-val* variant does not alter the levels or the synaptic localisation of this co-receptor.

***Lrp6-val* causes progressive synaptic defects with age**

Spine formation and growth are modulated by Wnt signalling in the hippocampus (*18*, *19*, *23*, *36*). Given that expression of *LRP6-Val* failed to stimulate spine growth and induced spine loss in cultured neurons (**Figures 1E and 1F**), we examined the *in vivo* impact of *Lrp6-val* on these post-synaptic structures. We analysed dendritic spines on the apical dendrites of CA1 pyramidal neurons in adult *Lrp6-val* knock-in mice crossed to a *Thy1-GFP* expressing line (*37*) (**Figure 2B**). Although no differences in spine density were observed, spine head width was reduced in *Lrp6-val* mice compared to WT mice at 7-9 months (**Figures 2C and 2D**). Thus, adult mice carrying the *Lrp6-val* variant display impaired spine growth.

Given our data on the synaptic localisation of LRP6 and the role of Wnt signalling in synaptic function (*38*, *39*), we examined synaptic transmission in the *Lrp6-val* mice at Schaffer collateral (SC)-CA1 synapses, where deficient Wnt signalling leads to defects in synaptic transmission (*12*). Evoked excitatory post-synaptic currents (EPSCs), in response to SC stimulation of increasing intensity (input-output (I/O) curve), were recorded in CA1 pyramidal cells at 7-9 months. No significant differences were observed between WT and *Lrp6-val* mice even at high stimulation intensities (**Figures S3A and S3B**), suggesting that basal synaptic transmission at SC-CA1 synapses is unaffected by the presence of the *Lrp6-val* variant at this age.

Wnt signalling deficient mice exhibit reduced neurotransmitter release probability (*22*, *40*). We therefore investigated possible defects in neurotransmitter release. EPSCs evoked at brief intervals at SC-CA1 synapses were recorded from WT and *Lrp6-val* mice at 7-9 months. We analysed the paired pulse ratio (PPR), which depends on presynaptic short-term plasticity mechanisms and is inversely correlated with release probability (*41*, *42*). *Lrp6-val* mice exhibited increased PPRs compared to WT mice at 50 ms inter-stimulus intervals (ISI), consistent with a reduced release probability at 7-9 months (**Figures 2E and 2F**). Thus, neurotransmitter release is compromised in adult *Lrp6-val* mice.

Given that cKO mice for *Lrp6* exhibit age-dependent synaptic deficits (*13*), we interrogated whether synaptic defects become more pronounced with age. We evaluated dendritic spines in older *Lrp6-val;Thy1-GFP* mice (**Figure 3A**). Our analyses revealed a significant decrease in both spine density and head width in *Lrp6-val* mice compared to WT mice at 12-14 months (**Figure 3B**). Given that spine size but not spine number was affected in 7-9-month-old *Lrp6-val* mice, these results demonstrate that spine deficits become more severe with age.

Next, we evaluated basal synaptic transmission in 12-month-old mice by performing I/O curve recordings in hippocampal slices. Interestingly, the amplitude of evoked EPSCs were significantly smaller in 12-month-old *Lrp6-val* mice compared to WT mice at all stimulus intensities (**Figures 3C and 3D**). Thus, the *Lrp6-val* variant impairs basal synaptic transmission at this age but not at 7-9 months (**Figures S3A and S3B**). We then measured neurotransmitter release probability and found that the PPR was significantly higher in *Lrp6-val* mice compared to WT mice at both 50 and 100 ms ISI, consistent with a reduction in release probability (**Figures 3E and 3F**). Given that PPR was significantly higher at 50 ms but not at 100 ms ISI in *Lrp6-val* mice at 7-9 months, these results suggest that defects in neurotransmitter release are more pronounced in older animals.

To further define the role of *Lrp6-val* in neurotransmitter release at 12 months, we recorded responses to a 3 second high-frequency stimulus train (20Hz), which fully depletes presynaptic terminals of the readily releasable pool (RRP) (*43*). Using first order correction for vesicle recycling (*43*), a significant reduction in the size of the RRP was observed in 12-month-old *Lrp6-val* mice when compared to WT mice (**Figures 3G, 3H and 3I**). However, synaptic vesicle fusion efficiency and recycling rate were unaffected (**Figure S3C**), suggesting that the defect in release probability is due to a reduced RRP.

The defects in vesicular release probability at 12 months suggested potential structural changes at presynaptic terminals of *Lrp6-val* mice. To investigate this hypothesis, we evaluated the number and size of presynaptic boutons using the presynaptic marker, vGlut1, in the CA1 stratum radiatum (SR) of *Lrp6-val* mice at 12-14 months (**Figure 4A**). Indeed, *Lrp6-val* mice had smaller and fewer vGlut1 puncta compared to WT mice

(**Figure 4B**). As *Lrp6-val* mice exhibited deficits in synaptic vesicle release, due to a smaller RRP (**Figure 3**), we assessed possible ultrastructural changes by electron microscopy (EM). We observed fewer synaptic vesicles at presynaptic terminals, but no differences in the length of the post-synaptic density (PSD) at SC-CA1 synapses of *Lrp6-val* mice (**Figures 4C and 4D**). These findings indicate that impaired neurotransmitter release in *Lrp6-val* mice is due to a reduction in synaptic vesicle number, consistent with a reduced RRP.

Given that defects at the pre- and post-synaptic sites were exacerbated with age in *Lrp6-val* mice, we compared the number of excitatory synapses at the different ages. Synapses were quantified based on the co-localisation of Bassoon and Homer1, pre- and post-synaptic markers respectively, in the CA1 SR region. At 7-9 months and 12 months, no differences were observed between WT and *Lrp6-val* mice (**Figures 5A-5D**). However, a significant reduction in the number of excitatory synapses was detected at 16-18 months in *Lrp6-val* mice when compared to WT mice (**Figures 5E and 5F**). Due to the age of these animals, we examined possible neuronal loss, which could affect synapse number, in the stratum pyramidale layer using DAPI and NeuN (**Figure S4A**). No difference in the percentage of NeuN positive cells was identified between WT and *Lrp6-val* mice at 16-18 months (**Figure S4B**). Thus, the *Lrp6-val* variant confers increased synaptic vulnerability as animals age, a process that is not due to changes in neuronal number.

As the *Lrp6-val* variant is predominantly present as heterozygous in the human population (*30*), we also analysed heterozygous *Lrp6-val* mice at 12-14 months. Although no differences were detected in the presynaptic marker vGlut1 between WT and heterozygous mice, homozygous mice exhibited a reduction in vGlut1 puncta number (**Figure S5A**). Post-synaptically, both heterozygous and homozygous *Lrp6-val* mice exhibited a decrease in the number and size of dendritic spines when compared to WT mice (**Figure S5B**). Thus, carrying one allele of the *Lrp6-val* confers postsynaptic vulnerability.

Wnt signalling is impaired in *Lrp6-val* mice and *Lrp6-val* neurons do not respond to Wnt7a

To begin addressing the molecular mechanisms through which aged *Lrp6-val* mice exhibit synaptic defects, we investigated if canonical Wnt signalling was affected in aged mice. We therefore evaluated the mRNA levels of *Axin2,* a target of canonical Wnt signalling (*44*) (**Figure S6A**). *Axin2* expression was not affected in 4–7-month-old *Lrp6-val* mice (**Figure S6B**), but it was significantly decreased in 12-15-month-old *Lrp6-val* mice compared to WT (**Figure S6C**). Thus, Wnt signalling is compromised with age in *Lrp6-val* mice*,* consistent with the appearance of synapse defects.

The above findings led us to hypothesize that the LRP6-Val receptor does not signal properly. We therefore interrogated if neurons from *Lrp6-val* mice responded to exogenous Wnts (**Figures 6A**). Previous studies demonstrate that Wnt7a promotes the formation of excitatory synapses in hippocampal neurons (*15–18*). Consistently, Wnt7a significantly increased the number of synapses in neurons from WT mice compared to neurons exposed to a control vehicle (veh) (**Figures 6B and 6C**). However, Wnt7a was unable to increase synapse number in hippocampal neurons from *Lrp6-val* mice (**Figures 6B and 6C**). Crucially, the same effect was observed with a second concentration of Wnt7a (**Figures S7A and S7B**). Next, we examined if neurons from *Lrp6-val* mice respond to Wnt3a, another ligand involved in presynaptic assembly (*16*, *45*). Moreover, the Ile to Val amino acid substitution in *LRP6* is in the Wnt3a binding site (*31–33*) and that expression of *LRP6-Val* in a cell line reduces Wnt3a-mediated signalling (*28*). We found that Wnt3a increased the number of synapses in WT neurons but failed to increase synapse number in *Lrp6-val* neurons (**Figures S7A and S7C**). Thus, *Lrp6-val* neurons respond to neither Wnt7a or Wnt3a. The lack of response to Wnt ligands was not due to decreased levels of the LRP6-Val receptor at the plasma membrane, as the surface levels of LRP6 were the same between WT and *Lrp6-val* neurons (**Figures S7A, S7D and S7E**). Thus, *Lrp6-val* impairs the ability of neurons to respond to exogenous Wnt ligands without affecting its surface localisation.

LRP6-Val impairs the formation of the Wnt7a-induced LRP6-Fz5 complex and downstream signalling

The lack of response to Wnt7a and Wnt3a in neurons from *Lrp6-val* mice suggested that the presence of LRP6-Val could impair the formation of a complex between LRP6 and Frizzled (Fz) receptors, which is crucial for the activation of the canonical Wnt signalling pathway (*34*). We specifically chose to examine the interaction between Fz5 and LRP6 because this Fz receptor is required for Wnt7a-mediated presynaptic assembly in hippocampal neurons (*15*). We co-expressed *Fz5-HA* with WT *LRP6* or *LRP6-Val* in HeLa cells to evaluate their interaction, which is induced by Wnt7a, using proximity ligation assay (PLA), a technique that allows the detection of protein-protein interactions at less than 40nm in cells (*46*, *47*) (**Figure 6D**). The PLA signal was elevated in cells expressing *Fz5-HA* and WT *LRP6* or *LRP6-Val* when compared to control cells (**Figures 6E and 6F**). No differences in the interaction were observed between cells expressing *Fz5-HA* and WT *LRP6* or *LRP6-Val* under basal conditions (**Figures 6E, 6F and 6G**). In contrast, Wnt7a significantly increased the PLA signal intensity in cells expressing *Fz5-HA* and WT *LRP6* but not in cells expressing *Fz5-HA* and *LRP6-Val* (**Figures 6E and 6G**). These results were not due to changes in the surface levels of these receptors, as determined by surface biotinylation (**Figures S8A-S8E**). Together, these results demonstrate that the presence of LRP6-Val impairs the formation of the Wnt-induced LRP6-Fz receptor complex, which is required for signalling.

We next examined if downstream signalling was affected by the presence of LRP6-Val. The formation of LRP6-Fz complex promotes the intracellular phosphorylation of LRP6 at multiple sites, including at serine 1490, which is important for LRP6 function (*48*). We therefore tested if this posttranslational modification was affected by the LRP6-Val variant. Cells expressing WT *LRP6* and *Fz5-HA* or *LRP6-Val* and *Fz5-HA* were exposed to recombinant Wnt7a and the level of phosphorylated LRP6 (pLRP6) at serine 1490 was evaluated by immunofluorescence microscopy. As expected, Wnt7a significantly increased the level of pLRP6 in cells expressing WT *LRP6* (**Figures 6H and S8F**). However, no changes were observed in the pLRP6 levels in cells expressing the *LRP6-*

Val variant (**Figures 6H and S8F**). Thus, the presence of the LRP6-Val affects the formation of the LRP6-Fz5 complex and subsequent downstream signalling.

***Lrp6-val* does not affect plaque load in NL-G-F mice**

The findings that the *LRP6-Val* variant is associated with late-onset AD (*28*) and that conditional knockout of *Lrp6* in neurons of the APP/PS1 AD mouse model exacerbates the formation of Aβ plaques (*13*) led us to interrogate the impact of the *Lrp6-val* variant on amyloid pathology. We crossed the *Lrp6-val* mice to the *NL-G-F*, a knock-in AD mouse model that carries a humanized Aβ region of APP with three mutations associated with AD (*49*). In *NL-G-F* mice, plaque deposition begins around 2 months, with a significant increase in the number at 7 months (*49*). We assessed the impact of *Lrp6-val* on plaque load in homozygous *NL-G-F* mice. No differences in plaque burden were detected between *NL-G-F* and *NL-G-F;Lrp6-val* mice at 2 months, 7 months and 10 months (**Figures S9A-S9F**). Furthermore, Aβ coverage (area covered by Aβ) was unaltered in *NL-G-F;Lrp6-val* mice compared to *NL-G-F* mice at 7 months and 10 months (**Figures S9C-S9F**). Thus, the presence of the *Lrp6-val* variant does not exacerbate plaque load in *NL-G-F* mice at the ages examined.

Next, we examined the levels of soluble and insoluble Aβ42, as this peptide is the most abundant Aβ species in *NL-G-F* mice (*49*). However, no differences in the level of Aβ42 was observed between *NL-G-F* and *NL-G-F;Lrp6-val* mice at 10 months (**Figure S10**). These results are consistent with our findings that Aβ plaque number and Aβ coverage are unaffected in *NL-G-F* mice when carrying the *Lrp6-val* variant.

***Lrp6-val* exacerbates synapse loss in NL-G-F mice**

Although the impact of *Lrp6* cKO on Aβ plaque load has been examined in the context of AD (*13*), changes in synapse density were not investigated. Our findings that *Lrp6-val* mice exhibit synaptic defects led us to interrogate the contribution of this SNP to synapse vulnerability in AD. We therefore evaluated the impact of *Lrp6-val* on synapses in *NL-G-F* mice at 2 months of age, when plaques begin to form (*49*). However, no differences in

synapse number were observed between WT, *Lrp6-val*, *NL-G-F* and *NL-G-F;Lrp6-val* mice at this early stage (**Figures S11A and S11B**).

We next investigated the impact of the *Lrp6-val* variant on synapses at 7 months of age in *NL-G-F* mice, by which time a significant number of plaques are present (*49*). Given that synapse loss is particularly pronounced around Aβ plaques (*5–8*) (**Figure 7A**), synapse number was quantified at increasing distances from the centre of a plaque, or from a similar area in WT and *Lrp6-val* mice, in the CA1 SR (**Figure 7B**). At 0-10 µm from the centre of a plaque, a significant reduction in synapse number was observed in *NL-G-F* mice when compared to WT mice or to *Lrp6-val* mice (**Figures 7B and 7C**). A further decrease in synapse number was observed between *NL-G-F;Lrp6-val* double mutant mice when compared to *NL-G-F*, *Lrp6-val* or WT mice. This effect was also observed at further distances from the centre of a plaque (**Figures 7B and 7C**). Thus, carrying the *Lrp6-val* variant exacerbates synapse loss around plaques in *NL-G-F* mice.

To determine if the enhanced synapse degeneration at 7 months was due to deregulation of Wnt signalling components, we examined the expression of key Wnt ligands and receptors by qPCR in the hippocampi of WT, *Lrp6-val*, *NL-G-F* and *NL-G-F;Lrp6-val* mice. However, no differences were detected in the expression of Wnt receptors *Lrp6* and *Fz5* or the Wnt ligands *Wnt7a* and *Wnt7b* (**Figure S12**).

We also examined if synapse number was more pronounced in the double mutant mice when compared to *NL-G-F* mice at 10 months as Aβ pathology becomes more severe with age in *NL-G-F* mice (*49*). Interestingly, we found no significant differences in synapse loss around plaques between *NL-G-F* and *NL-G-F; Lrp6-val* mice at this age (**Figures S11C and S11D**). Together our results demonstrate that carrying the LRP6-Val receptor accelerates synapse loss in *NL-G-F* mice when synaptic defects become evident but not with progressive pathogenesis.

Discussion

Here, we evaluate the impact of the *LRP6-Val* variant, which is linked to LOAD, on synaptic connectivity during ageing and in AD. We generated a novel knock-in mouse model carrying this variant. Analyses of homozygous *Lrp6-val* mice reveal that this SNP induces age associated defects in synaptic transmission and neurotransmitter release. *Lrp6-val* mice also exhibit progressive structural synaptic defects in the hippocampus. Importantly, the presence of *Lrp6-val* exacerbates synapse loss around plaques in the *NL-G-F* AD model. Investigation into the molecular mechanisms underlying the synaptic defects elicited by LRP6-Val reveals a defect in the formation of the LRP6-Fz5 complex mediated by Wnt7a, which explains the decreased downstream signalling that is only evident with age. Thus, our studies also reveal a previously unrecognized molecular mechanism by which this variant impacts Wnt signalling and uncover a role for *LRP6-Val* in synapse degeneration in AD.

The LRP6 receptor, which localises to synapses, promotes the assembly of synapses. Using super-resolution microscopy, we found that LRP6 is present at both pre- and post-synaptic sites. Expression of WT *LRP6* in neurons increases the number of presynaptic puncta and promotes spine growth, consistent with activation of the Wnt pathway in neurons (*16*, *18*) and in agreement with a previous study showing that LRP6 localizes to both pre- and post-synaptic sites and is required for synaptogenesis in cultured neurons (*20*). In contrast, expression of the *LRP6-Val* variant in neurons neither increases the number of presynaptic sites nor affects spine size but induces spine loss. Together, these findings demonstrate that expression of the *LRP6-Val* variant in hippocampal neurons fails to promote synapse formation.

Homozygous *Lrp6-val* mice exhibit structural and functional synaptic defects that become more pronounced with age. At 7-9 months, we observe reduced spine head width without changes in spine number or synapse number, whereas at 12-14 months both spine number and head width and, the number of vGlut1 puncta are decreased. Moreover, defects in basal synaptic transmission and synaptic vesicle release, due to a smaller RRP, are exacerbated from 7-9 months to 12-14 months in homozygous *Lrp6-val* mice.

However, no changes in synapse number are observed at these ages. In contrast, homozygous *Lrp6-val* mice exhibit a reduced number of excitatory synapses at 16-18 months. Importantly, heterozygous *Lrp6-val* mice also exhibit synaptic defects, suggesting that carrying a single allele of this variant confers synaptic vulnerability.Thus, the presence of the LRP6-Val variant contributes to progressive synaptic dysfunction and synapse degeneration.

Multiple variants of *LRP6* have been linked to various age-associated diseases (*28*, *50*, *51*), including the *LRP6-Val* variant studied in this work, which has an allele frequency of 0.17 in the European population (*30*). First, *LRP6-Val* is associated with a 60% increase in bone fracture risk in older men (*50*). Second, *LRP6-Val* is a risk factor for carotid artery atherosclerosis in hypertensive patients over the age of 65 (*51*). Finally, *LRP6-Val* is associated with LOAD (*28*). Thus, carrying the LRP6-Val variant results in age-related phenotypes that extend beyond the nervous system.

What are the molecular mechanisms that contribute to synaptic defects in the *Lrp6-val* mice? The synaptic deficits in *Lrp6-val* mice are not due to defects in the levels or localisation of the LRP6-Val protein, as similar protein levels are found at synapses and at the cell surface when compared to wildtype LRP6. This finding suggests possible defects in downstream signalling. Consistent with this hypothesis, Wnt7a and Wnt3a fail to induce excitatory synapse formation in neurons isolated from *Lrp6-val* mice. This lack of response correlates with defects in the interaction between Fz5 and LRP6-Val in response to Wnt7a and reduced downstream Wnt signalling as determined by the levels of pLRP6 and the levels of *Axin2* expression at 12-15 months in *Lrp6-val* mice. Moreover, expression of *LRP6-Val* attenuates canonical Wnt signalling as evaluated by the TOPFlash assay (*28*). Thus, the presence of LRP6-Val impairs the formation of the Wnt receptor complex in response to Wnt7a, which decreases downstream signalling resulting in synaptic dysfunction and synapse degeneration.

The lack of response of *Lrp6-val* neurons to exogenous Wnt7a or Wnt3a suggests that LRP6-Val acts like a null mutant. Given that *Lrp6-val* mice do not display developmental defects, the phenotypes of the *Lrp6-val* mice does not phenocopy those observed in *Lrp6*

full KO mice, which die at birth due to severe embryonic defects (*52*). This functional difference could be due to different auxiliary proteins for the LRP6 co-receptor that compensate for signalling defects in the *Lrp6-val* mice during development but not in the adult brain.

The synaptic defects are manifested with age in the *Lrp6-val* mice. A possible explanation for this phenotype is that canonical Wnt signalling is dampened with age. Indeed, canonical Wnt signalling and several Wnt ligands, including Wnt7a, are reduced in the ageing brain (*53*, *54*). Based on these findings, we propose that reduced levels of Wnt proteins with age combined with the presence of a less functional receptor, such as LRP6-Val, contributes to the manifestation of age-dependent synapse loss in *Lrp6-val* mice.

In the context of AD, our studies demonstrate that carrying the *Lrp6-val* variant increases synapse vulnerability. Indeed, *Lrp6-val* exacerbates synapse loss surrounding plaques in the *NL-G-F* model at 7 months. This is not due to differential expression of Wnt components, increased Aβ42 levels or plaque load. Our findings are in contrast with those reported using the conditional KO of *Lrp6* crossed to the APP/PS1 AD model, which reported increased Aβ40 and Aβ42 levels and enhanced plaque load were observed (*13*). These differing results could be due to various reasons. First, our knock-in (KI) model contains a single amino acid substitution in the *Lrp6* gene, which is likely to result in a milder phenotype than that observed in the cKO model. Second, the cKO of *Lrp6* was studied in APP/PS1, a transgenic model that overexpresses mutant APP and Presenilin1 (*13*). In contrast, the *NL-G-F* is a KI model with normal levels of APP. Thus, increased synapse vulnerability in the *NL-G-F* model carrying the Lrp6val variant is not due to increased Aβ load.

Understanding how risk factors contribute to the pathogenesis of AD is critical for identifying therapeutic targets to prevent or ameliorate synaptic dysfunction and synapse loss in this condition. Our findings uncover, for the first time, the impact of a genetic variant of *LRP6* associated with LOAD on synapse vulnerability with age and in the context of AD. Thus, these findings further strengthen the link between deficient Wnt signalling and synapse loss in the ageing and AD brain.

Materials and Methods

Animals

Experiments with mice were carried out under personal and project licenses granted by the UK Home Office in accordance with the Animals (Scientific Procedures) Act 1986 and were approved by the UCL ethical committee. Animals were housed in ventilated cages with a 12-hour light-dark cycle and *ad libitum* access to food and water. Both male and female animals were used. Ages are specified in the figure legends.

Generation of *Lrp6-val* mutant mice

Single-strand oligonucleotides (ssODNs) were synthesised by Integrated DNA Technologies (IDT)(ssODN:CATCAGAGGCAGTCTCAGGCTGTGGCTTTGGAACATACCCTTTCTCGGGGTTTACCACAACGGCTCAGGTCTGTCTTGCTCGCCTTTTAGAACCACTCCAACTGATCGTCCATCTAATC). ssODNs were positioned adjacent to the gRNA site: ACAGACCTCGAGCCATTGTGG. gRNA oligonucleotides were synthesised, the two strands annealed and cloned using BsaI into a vector containing the gRNA backbone and a T7 promoter for RNA production. For Cas9 mRNA production, the vector from (*55*), was modified to contain the T7 promoter. 4-5-week-old C57BL/6NTac females were super-ovulated by injection of 5 IU of pregnant mare's serum (PMSG) and 48 hours later, 5 IU of human chorionic gonadotrophin (HCG) was injected. Females were mated with C57BL/6NTac males. Cumulus oocyte complexes were dissected from oviducts 21-22 hrs post HCG and treated with hyaluronidase. Fertilised 1-cell embryos were maintained at 37°C in KSOM media prior to cytoplasmic injection. 24-27 hrs post HCG, 50 ng/µl Cas9 mRNA, 25 ng/µl gRNA (each) and 100 ng/µl oligonucleotide were injected into the cytoplasm of fertilised 1-cell embryos held in FHM medium. Viable embryos were transferred on the same day by oviducal embryo transfer into 0.5 days post-coital pseudo-pregnant female F1 (CBA/C57BL/6J) recipients. Homozygous *Lrp6-Val* C57BL/6NTac mice were backcrossed to C57BL/6J mice.

Genotyping

Lrp6-val mice were crossed to the *Thy1-GFP* mice or *NL-G-F* model to obtain *Lrp6-val;Thy1-GFP* mice and *NL-G-F;Lrp6-val* mice respectively. Genotyping was performed on ear biopsies using the following primers: *Lrp6* WT Forward: GATACGTTGCTTTAATGCCTTTAGCAAGACAGACCTCGAGCAA, *Lrp6-val* Forward: TGGCGGCAAGACAGACCTCGAGCAG, *Lrp6* (WT and Val) Reverse: AACGCGCAACGAAGGGTGAGGAGGCATCA. *NL-G-F*: 5′-ATCTCGGAAGTGAAGATG-3′, 5′-ATCTCGGAAGTGAATCTA-3′, 5′-TGTAGATGAGAACTTAAC-3′ and 5′-CGTATAATGTATGCTATACGAAG-3′ (*49*). GFP: forward 5'-TCTGAGTGGCAAAGGACCTTAGG-3' and reverse 5'-CGCTGAACTTGTGGCCGTTTACG-3' (*37*).

Hippocampal culture and transfection

Rat hippocampal cultures were prepared from embryonic day 18 (E18) embryos from Sprague-Dawley rats as previously described (*12*, *19*). Cultures were maintained for 13-14 days in vitro (DIV) to assess presynaptic terminals or until 21 DIV to investigate dendritic spines or to analyse the impact of sFRP1 on presynaptic terminals.

Mouse hippocampal neurons were prepared from E15.5-E16.6 WT or *Lrp6-val* mice and maintained until 12-21 DIV. Neurons were treated with either 100ng/ml or 200 ng/ml recombinant Wnt7a (PeproTech, 120-31), with 200ng/ml recombinant Wnt3a (R&D systems) or with BSA (control vehicle) for 3 hours at on DIV for analyses of synapses.

Rat hippocampal neurons were either transfected using Amaxa nucleofection prior to or with calcium phosphate transfection at 7-9 DIV with DNA constructs expressing EGFP-actin, human *LRP6* WT or human *LRP6-Val* and MESD (mesoderm development LRP chaperone protein), which is required for maturation and trafficking of LRP6 (*56*). Control neurons were transfected with EGFP-actin only. Neurons (DIV 20) were treated with 1µg/ml recombinant sFRP1 (R&D systems) overnight for analyses of presynaptic terminals.

HeLa cell culture and transfection

HeLa cells were grown in DMEM (Gibco) supplemented with 10% FBS and 1% penicillin/streptomycin (Gibco) and maintained at 37°C and 5% CO_2. Cells were seeded

on 12mm glass coverslips at a density of $13.4x10^4$ cells/cm^2 for PLA assays and for analyses of pLRP6 and at $18.6x10^4$ cells/cm^2 for surface biotinylation.

Cells were transfected with plasmids encoding EGFP, Fz5-HA, MESD and *LRP6* WT or *LRP6-Val* using Lipofectamine 3000 (Invitrogen) and OPTIMEM for 4 hrs according to the manufacturer's protocol,. The transfection medium was then replaced with OPTIMEM. 48hr post transfection, cells were treated with serum free DMEM containing recombinant Wnt7a (200 ng/ml, PreproTech, 120-31) or BSA (control) for 30 or 60 minutes.

List of plasmids

LRP6 WT (Addgene plasmid # 27242) and Fz5-HA were gifts from Professor Xi He. MESD-Flag was a gift from Professor B. Holdener. EGFP-actin was a gift from Dr Y. Goda. *LRP6-Val-HA* was a gift from Professor R. T. Moon. The untagged *LRP6-Val* plasmid used in this paper was generated using constructs kindly provided by Professor R. T. Moon.

Brain section preparation

For cryostat sections used for immunostaining, 4% paraformaldehyde (PFA) fixed brains were immersed in 30% sucrose and frozen in precooled 2-methylbutane. 30-50µm sagittal sections were cut using a cryostat and stored at -20°C. Vibratome sections were prepared as previously described (*57*). Briefly, brains were rapidly dissected, immersed in artificial cerebrospinal fluid (aCSF) and 250-300µm thick sagittal brain slices were cut. Then, slices were fixed in 4% PFA/ 4% sucrose in PBS.

Immunofluorescence staining

Immunofluorescence staining was performed as previously described (*57*). Slices were permeabilized and blocked in 0.5% Triton-X-100 + 10% donkey serum in PBS for 3-4 hours at room temperature and then incubated with primary antibodies overnight at 4°C. Secondary antibodies (1:500; Alexa Fluor, Invitrogen) were incubated for 2 hours at room temperature. Slices were incubated in DAPI, washed with PBS and mounted with Fluoromount-G (SouthernBiotech).

Cultured hippocampal neurons were fixed in 4% PFA with 4% sucrose in PBS for 20 minutes at room temperature. Neurons were permeabilized in 0.05% Triton-X-100 in PBS for 5 minutes, blocked in 5% BSA for 1 hour, both at room temperature, and then incubated with primary antibodies overnight at 4ºC. Secondary antibodies (1:600; Alexa Fluor, Invitrogen) were incubated for 1 hour at room temperature. Neurons were incubated with DAPI, washed with PBS and mounted with FluorSave (Millipore).

Proximity ligation assay (PLA)

Proximity ligation assay was performed according to the manufacturer's protocol (Sigma Aldrich). Briefly, cells were washed with PBS, fixed with warm 4% PFA for 15 minutes then blocked for 60 minutes at 37°C with the Duolink Blocking solution. Cells were incubated overnight at 4°C with Anti-LRP6 (R&D, AF1505) and anti-HA (Sigma, H6908) primary antibodies in Duolink Antibody diluent solution (1:800). Cells were washed three times with the Duolink Wash Buffer A and incubated with the anti-rabbit MINUS and anti-goat PLUS PLA probes in Duolink Antibody diluent solution for 1 hour at 37°C. After two washes in Wash Buffer A, cells were incubated with the Duolink Ligation solution for 30 minutes at 37°C. After another two Wash Buffer A washes, cells were incubated with the Duolink Amplification solution for 1 hour 40 minutes at 37°C. Cells were washed 2x10 minutes in Wash Buffer B and for 1 minute in 0.01x Wash Buffer B. Cells were then permeabilised for 10 minutes with 0.1% Triton/PBS and blocked in 5% BSA for 1 hour. Anti-GFP (1:500, Millipore, 06-896) primary antibody was added for 1 hour at RT, followed by 3 PBS washes and the addition of AlexaFluor 488 chicken for 1 hour at RT. After 3x PBS washes, coverslips were mounted using 5µl per coverslip of Duolink In Situ Mounting Medium with DAPI.

List of primary antibodies

APP (6E10) (Novus Biotech, NBP2-62566, RRID:AB_2917960), Amyloid-β (BioLegend, 803001, RRID:AB_2564653), β-Actin (Cell Signalling Technology, 4970, RRID:AB_2223172), Bassoon (Novus Biologicals, NB120-13249), Bassoon (Synaptic systems, 141016, RRID:AB_2661779), GFP (Millipore, 06-896, RRID:AB_310288), GFP (Invitrogen, A-6455), HA (Sigma, H6908, RRID:AB_260070), HA (Roche, 11867423001, RRID:AB_390918), Homer1, (Synaptic systems, 160002, RRID:AB_2120990), Homer1,

(Synaptic systems, 160003, RRID:AB_887730), Homer1, (Synaptic systems, 160006, RRID:AB_263122), LRP6 (Abcam, ab134146, RRID:AB_2895164), LRP6 (R&D, AF1505, RRID:AB_2266025), LRP6 (Cell Signalling Technology, 2560, RRID:AB_2139329), LRP6 (Cell Signalling Technology, 3395, RRID:AB_1950408), pLRP6 (Cell Signalling Technology, 2568, RRID:AB_2139327), MAP2 (Abcam, ab5392, RRID:AB_2138153), MAP2 (Abcam, ab92434, RRID:AB_2138147), NeuN, (Cell Signalling Technology, 12943, RRID:AB_2630395), PSD-95 (Millipore, MAB1598, RRID:AB_94278), α-Tubulin (Sigma, T9026, RRID:AB_477593), vGlut1 (Millipore, AB5905, RRID:AB_2301751), Vinculin (Sigma, V4505, RRID:AB_477617).

Confocal microscopy

Images were acquired on a Leica SP8 or an Olympus FV1000 inverted confocal microscope. For analyses of synaptic puncta and dendritic spines in brain sections, 3 images (stacks) were acquired per brain section and 3 brain sections were analysed per animal. For hippocampal cultures, 6-13 images (stacks) were acquired per condition. Each stack comprised 8-11 equidistant planes, 0.2-0.25µm apart, and were acquired using a 63x 1.40 NA oil objective. For analyses of NeuN staining, a stack of 31 equidistant planes, 0.5µm apart, was acquired for each brain section with a 10x 0.40 NA objective on a Leica SP8. For plaque analyses of 2-month-old-mice, images were acquired on a Leica SP5. For each brain section, one stack of 25 equidistant planes, 0.99µm apart, was acquired using a 10x 0.30 NA objective. For analyses of plaques in 7 and 10-month-old-mice, a tile scan per brain section was acquired with a 20x 0.75 NA objective on a Leica SP8. Each stack comprised 59 equidistant planes for 7-month-old-mice and 144 equidistant planes for 10-month-old-mice, 0.35µm apart. For the PLA experiments and analyses of pLRP6 in HeLa cells, stacks of 9-10 equidistant planes with a z step of 0.5µm were acquired using a 40x oil objective on a Leica SP8. Two to three coverslips per experimental condition were imaged with 2-5 images per coverslip acquired.

SIM

Structured Illumination Microscopy (SIM) was performed on a Zeiss Elyra S.1 microscope with a 63x oil-immersion objective (NA 1.40). A z-stack of 15-20 equidistant planes were

acquired. For each field of view, nine images were acquired, using three different rotations and phases of structured illumination (a grid pattern) on the sample.

EM

Sagittal brain sections of 200 µm thickness, were cut on a vibratome then fixed in 2 % PFA/2.5 % Glutaraldehyde solution overnight at 4ºC. Samples were post-fixed in 1 % OsO_4 for 1 hr at 4ºC and stained with 1 % thiocarbohydrazide for 20 minutes at RT, 2 % OsO_4 for 30mins at RT, 1 % uranyl acetate (UA) ON at 4ºC and lead aspartate for 30 minutes at 60ºC. Next, slices were dehydrated in graded alcohol and embedded in resin. Ultra-thin sections (70 nm) were then cut using a diamond ultra 45-degree knife (Diatome) on a Leica UC7 ultramicrotome and collected on 2 x 1 mm slot grids. Images were acquired on a transmission electron microscope (T12 Tecnai Spirit Bio-Twin, FEI) each covering 5.8 μm^2 at 0.77 nm/pixel.

Image analyses

Image analyses were performed using Volocity software (Perkin Elmer). For hippocampal cultures and brain sections, customized thresholding protocols were used to detect pre- and postsynaptic puncta. Synapses were quantified as co-localized pre- and post-synaptic puncta. Analyses of dendrite spines was performed blind to the genotype or treatment. Dendritic spines were measured manually along 3-4 sections of dendrite. Spine size was quantified using the line tool by measuring the maximum spine head width. For the PLA experiment, only transfected cells were selected (based on GFP signal) and the total PLA signal intensity was quantified and divided by the number of cells analysed. For analyses of pLRP6 levels, cells expressing GFP and *LRP6* were analysed. Total pLRP6 intensity was normalised to total LRP6 intensity in each cell. For SIM images, synapses were identified manually and the co-localisation of LRP6 with synaptic markers was determined using Volocity. For neuronal number, the number of NeuN and DAPI positive cells were quantified using Volocity and divided by the total number of DAPI positive cells. In *NL-G-F* and *NL-G-F;Lrp6-val* mice, plaques were manually counted at 2 months, blind to the genotype.

At 7 months, plaque analyses were performed, blind to the genotype, using Fiji as previously described (*58*). Images were thresholded and then the % area was measured. The particle analysis tool was used to count the number of plaques. For EM, high-magnification images were used to manually count synaptic vesicles within 200 nm of the active zone. PSD length was quantified using a line tool in Fiji. Vesicle number was normalised to PSD length.

Electrophysiological Recordings

Electrophysiological recordings were performed in 7-8-month-old and in 12-13-month-old male and female mice. Acute transverse hippocampal slices (300 µm thick) from WT control mice and homozygous *Lrp6-val* mice were cut with a Leica VT-1000 vibratome in ice-cold artificial cerebrospinal fluid (ACSF) bubbled with 95% O_2/5% CO_2 containing: NaCl (125 mM), KCl (2.4 mM), $NaHCO_3$ (26 mM), NaH_2PO_4 (1.4 mM), D-(+)-Glucose (20 mM), $CaCl_2$ (0.5 mM) and $MgCl_2$ (3 mM). Brain slices from 12-13 months old mice were then transferred for 5 minutes into a series of three different oxygenated (95% O_2/5% CO_2) chambers in the same ACSF base but with gradual temperature and component variations: 1) 21 °C, $MgCl_2$ (1 mM) and $CaCl_2$ (0.5 mM) then placed at 36 °C for 5 minutes; 2) 36 °C, $MgCl_2$ (1 mM) and $CaCl_2$ (1 mM); and 3) 36 °C with $MgCl_2$ (1 mM) and $CaCl_2$ (2 mM) before cooling to 21 °C for at least 1 hour before recordings. Brain slices were placed in a chamber on an upright microscope and constantly perfused with NaCl (125 mM), KCl (2.4 mM), $NaHCO_3$ (26 mM), NaH_2PO_4 (1.4 mM), D-(+)-Glucose (20 mM), $MgCl_2$ (1 mM) and $CaCl_2$ (2 mM) supplemented with 10 µM bicuculline, to block GABA currents, at room temperature.

Whole-cell patch-clamp recordings were made from pyramidal cells in the CA1 region voltage-clamped at -60mV using patch pipettes with a resistance of 4-8 MΩ when filled with a caesium gluconate pipette solution composed of: D-gluconic acid lactone (130 mM), Hepes (10 mM), EGTA (10 mM), NaCl (10 mM), $CaCl_2$ (0.5 mM), $MgCl_2$ (1 mM), ATP (1 mM) and GTP (0.5 mM), QX314 (5 mM) adjusted to pH 7.2 with CsOH. To evoke postsynaptic currents, a bipolar concentric stimulating electrode (FHC) connected to a Grass S48 stimulator was placed around 100-200 µm from the patched cell. Cell input-output recordings were made with the stimulus pulse varied between 9 and 50V with a pulse width of 0.1 ms and delivered at a rate of 0.1 Hz. At least three responses per

stimulus intensity were averaged per cell. Paired pulse ratio (PPR) stimuli were delivered at a rate of 0.2 Hz with varying inter-stimulus intervals, ranging from 50 ms to 200 ms. Stimulus intensity was adjusted for each cell to elicit ~50% of the maximal response. PPR was calculated as the ratio of the peak amplitude of the second response over the first response and at least seven responses were averaged per cell for each inter-stimulus interval. For RRP size, initial fusion efficiency, and SV recycling rate calculation, CA1 cell EPSCs were recorded in response to 3 s duration trains of stimulation at 20 Hz and estimated as previously described (*40*, *43*).

The following two equations were used to estimate RRP size, fusion efficiency (*fe*), and vesicle recycling rate (α) using cumulative charge (*43*) in analysis of 20 Hz stimulus-evoked trains of EPSCs:

Equation1: fe=r(1)r(∞)(1−exp(−αΔt))fe=r(1)r(∞)(1−exp(−αΔt))

Equation2: fe=r(1)∑si=1r(i)exp(−α(S−i)Δt)fe=r(1)∑i=1sr(i)exp(−α(S−i)Δt)

r(1) is the charge of the first EPSC in the train, *r*(*i*) is the charge passed by the *i*th EPSC, *r*(∞) was calculated from the average charge of the last 10 EPSCs in the train, and Δ*t* is the stimulus interval in the train. The RRP was estimated as RRP = *r*(1)/*fe*.

Currents were recorded using an Axopatch 200B amplifier and low-pass filtered at 1 kHz and digitized at 10 kHz. Online monitoring of the data was performed using WinEDR and offline analysis using both WinEDR and WinWCP software (freely available online at http://spider.science.strath.ac.uk/sipbs/software_ses.htm).

Surface biotinylation and Western Blots

Surface biotinylation was performed using Sulfo-NHS-LC-LC biotin (Thermo, EZ-Link Sulfo NHS-LC-LC-Biotin) and streptavidin-agarose beads (Thermo Fisher). Samples were run on an 8% SDS-PAGE gel. Hippocampal homogenates from WT and *Lrp6-val* mice at 4 months old were resolved on 8-12 % SDS-PAGE gels. Two bands were observed for Fz5-HA. Both bands were quantified as this is likely due to changes in glycosylation of this receptor at the surface (*59*).

ELISA

NL-G-F and *NL-G-F;Lrp6-val* hippocampal tissue was homogenized in RIPA, followed by guanidine hydrochloride (GuHCL). Aβ42 peptides were quantified using the human Aβ 1-42 ELISA kit (WAKO) following the manufacturer's instructions.

Quantitative PCR (qPCR)

RNA was extracted from frozen hippocampal tissue using Trizol (Life Technologies) and the Direct-zol RNA MiniPrep Kit (Zymo Research), following the manufacturer's instructions. First-strand cDNA synthesis was performed with the RevertAid H Minus First Strand cDNA Synthesis kit (Thermo Fisher Scientific), following manufacturer's instructions. Quantitative PCR (qPCR) was performed using GoTaq qPCR Master Mix (Promega). *Gapdh*, *Canx*, or *Rpl13a* were used as housekeeping genes. The following primers were used. *Lrp6*: forward 5'-TCTTGTGGTTGTCTGGTGTGGAG-3' and reverse 5'-AGAAGACATATCAGAAAATGCAGGAGG-3' or forward 5'-AAGCTGCTGGAGAATGGAAA-3' and reverse 5'- CCAAAGAAATTCGCCTCAAG-3'. *Axin2*: forward '5- GAGGGACAGGAACCACTCG-3' and reverse: '5-TGCCAGTTTCTTTGGCTCTT-3'. *Fz5*: forward 5'- ACATGGAACGATTCCGCTAC-3' and reverse 5'- TCCCAGTGACACACACAGGT-3'. *Wnt7a*: forward 5'-TTTCTCAGCCTGGGCATAGT-3' and reverse 5'- CCAGAGCTACCACCGAAGAG-3'. *Wnt7b*: forward 5'- GCCTTCACCTATGCCATCAC-3' and reverse 5'-CCTTCCGCCTGGTTGTAGTA-3'. *Gapdh:* forward 5'-CGTCCCGTAGACAAAATGGT-3' and reverse 5'-TCAATGAAGGGGTCGTTGAT-3' or forward 5'-AGACAGCCGCATCTTCTTGT-3' and reverse 5'-CTTGCCGTGGGTAGAGTCAT-3'. *Canx*: forward 5'- CCCACATAGGAGGTCTGACA-3' and reverse 5'-GCTAGGAATGGAGGAGATCCA-3'. *Rpl13a*: forward 5'- GACTCCTGGTGTGAACCCA-3' and reverse 5'- CTCTACCCACAGGAGCAGT-3'.

Statistical analyses

All results are presented as mean ± SEM. Statistical analyses were performed in GraphPad Prism (Version 9) or SPSS (IBM, Version 27). Normality was assessed with Shapiro-Wilk or Kolmogorov-Smirnov tests. Normally distributed data was analyzed using T-tests for two conditions, one-way ANOVA for two or more conditions, or two-way

ANOVA for experiments with two independent variables. Post hoc tests are detailed in the figure legends. Non-normally distributed data was analyzed with non-parametric tests such as Kruskal-Wallis or Mann-Whitney. Statistical significance was accepted as * $p < 0.05$, ** $p < 0.01$, *** $p < 0.001$.

References

1. R. D. Terry *et al.*, Physical basis of cognitive alterations in Alzheimer's disease: synapse loss is the major correlate of cognitive impairment. *Ann. Neurol.* **30**, 572–580 (1991).
2. S. W. Scheff, D. A. Price, Alzheimer's disease-related alterations in synaptic density: neocortex and hippocampus. *J. Alzheimers Dis.* **9**, 101–115 (2006).
3. G. M. Shankar, D. M. Walsh, Alzheimer's disease: synaptic dysfunction and Abeta. *Mol. Neurodegener.* **4**, 48 (2009).
4. L. Mucke, D. J. Selkoe, Neurotoxicity of amyloid β-protein: synaptic and network dysfunction. *Cold Spring Harb. Perspect. Med.* **2**, a006338 (2012).
5. R. M. Koffie *et al.*, Apolipoprotein E4 effects in Alzheimer's disease are mediated by synaptotoxic oligomeric amyloid-β. *Brain*. **135**, 2155–2168 (2012).
6. R. M. Koffie *et al.*, Oligomeric amyloid beta associates with postsynaptic densities and correlates with excitatory synapse loss near senile plaques. *Proc. Natl. Acad. Sci. USA*. **106**, 4012–4017 (2009).
7. R. J. Jackson *et al.*, Human tau increases amyloid β plaque size but not amyloid β-mediated synapse loss in a novel mouse model of Alzheimer's disease. *Eur. J. Neurosci.* **44**, 3056–3066 (2016).
8. H. Dong, M. V. Martin, S. Chambers, J. G. Csernansky, Spatial relationship between synapse loss and beta-amyloid deposition in Tg2576 mice. *J. Comp. Neurol.* **500**, 311–321 (2007).
9. D. J. Selkoe, J. Hardy, The amyloid hypothesis of Alzheimer's disease at 25 years. *EMBO Mol. Med.* **8**, 595–608 (2016).
10. Y.-C. Lin, A. J. Koleske, Mechanisms of synapse and dendrite maintenance and their disruption in psychiatric and neurodegenerative disorders. *Annu. Rev. Neurosci.* **33**, 349–378 (2010).

11. Y. Chen, A. K. Y. Fu, N. Y. Ip, Synaptic dysfunction in Alzheimer's disease: Mechanisms and therapeutic strategies. *Pharmacol. Ther.* **195**, 186–198 (2019).
12. A. Marzo *et al.*, Reversal of synapse degeneration by restoring wnt signaling in the adult hippocampus. *Curr. Biol.* **26**, 2551–2561 (2016).
13. C.-C. Liu *et al.*, Deficiency in LRP6-mediated Wnt signaling contributes to synaptic abnormalities and amyloid pathology in Alzheimer's disease. *Neuron*. **84**, 63–77 (2014).
14. S. A. Purro, E. M. Dickins, P. C. Salinas, The secreted Wnt antagonist Dickkopf-1 is required for amyloid β-mediated synaptic loss. *J. Neurosci.* **32**, 3492–3498 (2012).
15. M. Sahores, A. Gibb, P. C. Salinas, Frizzled-5, a receptor for the synaptic organizer Wnt7a, regulates activity-mediated synaptogenesis. *Development*. **137**, 2215–2225 (2010).
16. E. K. Davis, Y. Zou, A. Ghosh, Wnts acting through canonical and noncanonical signaling pathways exert opposite effects on hippocampal synapse formation. *Neural Dev.* **3**, 32 (2008).
17. W. Cerpa *et al.*, Wnt-7a modulates the synaptic vesicle cycle and synaptic transmission in hippocampal neurons. *J. Biol. Chem.* **283**, 5918–5927 (2008).
18. L. Ciani *et al.*, Wnt7a signaling promotes dendritic spine growth and synaptic strength through Ca^{2+}/Calmodulin-dependent protein kinase II. *Proc. Natl. Acad. Sci. USA*. **108**, 10732–10737 (2011).
19. F. McLeod *et al.*, Wnt Signaling Mediates LTP-Dependent Spine Plasticity and AMPAR Localization through Frizzled-7 Receptors. *Cell Rep.* **23**, 1060–1071 (2018).
20. K. Sharma *et al.*, High-throughput genetic screen for synaptogenic factors: identification of LRP6 as critical for excitatory synapse development. *Cell Rep.* **5**, 1330–1341 (2013).
21. S. Fazel Darbandi *et al.*, Enhancing WNT signaling restores cortical neuronal spine maturation and synaptogenesis in tbr1 mutants. *Cell Rep.* **31**, 107495 (2020).

22. S. Galli *et al.*, Deficient Wnt signalling triggers striatal synaptic degeneration and impaired motor behaviour in adult mice. *Nat. Commun.* **5**, 4992 (2014).
23. C.-M. Chen *et al.*, Wnt5a is essential for hippocampal dendritic maintenance and spatial learning and memory in adult mice. *Proc. Natl. Acad. Sci. USA*. **114**, E619–E628 (2017).
24. A. Caricasole *et al.*, Induction of Dickkopf-1, a negative modulator of the Wnt pathway, is associated with neuronal degeneration in Alzheimer's brain. *J. Neurosci.* **24**, 6021–6027 (2004).
25. M. C. Rosi *et al.*, Increased Dickkopf-1 expression in transgenic mouse models of neurodegenerative disease. *J. Neurochem.* **112**, 1539–1551 (2010).
26. K. J. Sellers *et al.*, Amyloid β synaptotoxicity is Wnt-PCP dependent and blocked by fasudil. *Alzheimers Dement.* **14**, 306–317 (2018).
27. R. Killick *et al.*, Clusterin regulates β-amyloid toxicity via Dickkopf-1-driven induction of the wnt-PCP-JNK pathway. *Mol. Psychiatry*. **19**, 88–98 (2014).
28. G. V. De Ferrari *et al.*, Common genetic variation within the low-density lipoprotein receptor-related protein 6 and late-onset Alzheimer's disease. *Proc. Natl. Acad. Sci. USA*. **104**, 9434–9439 (2007).
29. M. A. Alarcón *et al.*, A novel functional low-density lipoprotein receptor-related protein 6 gene alternative splice variant is associated with Alzheimer's disease. *Neurobiol. Aging*. **34**, 1709.e9–18 (2013).
30. 1000 Genomes Project Consortium *et al.*, A global reference for human genetic variation. *Nature*. **526**, 68–74 (2015).
31. E. Bourhis *et al.*, Reconstitution of a frizzled8.Wnt3a.LRP6 signaling complex reveals multiple Wnt and Dkk1 binding sites on LRP6. *J. Biol. Chem.* **285**, 9172–9179 (2010).
32. S. Chen *et al.*, Structural and functional studies of LRP6 ectodomain reveal a platform for Wnt signaling. *Dev. Cell*. **21**, 848–861 (2011).
33. H. Hirai, K. Matoba, E. Mihara, T. Arimori, J. Takagi, Crystal structure of a mammalian Wnt-frizzled complex. *Nat. Struct. Mol. Biol.* **26**, 372–379 (2019).

34. Y. Hua *et al.*, Oligomerization of Frizzled and LRP5/6 protein initiates intracellular signaling for the canonical WNT/β-catenin pathway. *J. Biol. Chem.* **293**, 19710–19724 (2018).
35. B. Mao *et al.*, LDL-receptor-related protein 6 is a receptor for Dickkopf proteins. *Nature*. **411**, 321–325 (2001).
36. E. Ramos-Fernández, C. Tapia-Rojas, V. T. Ramírez, N. C. Inestrosa, Wnt-7a Stimulates Dendritic Spine Morphogenesis and PSD-95 Expression Through Canonical Signaling. *Mol. Neurobiol.* **56**, 1870–1882 (2019).
37. G. Feng *et al.*, Imaging neuronal subsets in transgenic mice expressing multiple spectral variants of GFP. *Neuron*. **28**, 41–51 (2000).
38. F. McLeod, P. C. Salinas, Wnt proteins as modulators of synaptic plasticity. *Curr. Opin. Neurobiol.* **53**, 90–95 (2018).
39. C. A. Oliva, C. Montecinos-Oliva, N. C. Inestrosa, Wnt signaling in the central nervous system: new insights in health and disease. *Prog Mol Biol Transl Sci*. **153**, 81–130 (2018).
40. L. Ciani *et al.*, Wnt signalling tunes neurotransmitter release by directly targeting Synaptotagmin-1. *Nat. Commun.* **6**, 8302 (2015).
41. L. E. Dobrunz, C. F. Stevens, Heterogeneity of release probability, facilitation, and depletion at central synapses. *Neuron*. **18**, 995–1008 (1997).
42. D. Fioravante, W. G. Regehr, Short-term forms of presynaptic plasticity. *Curr. Opin. Neurobiol.* **21**, 269–274 (2011).
43. J. F. Wesseling, D. C. Lo, Limit on the role of activity in controlling the release-ready supply of synaptic vesicles. *J. Neurosci.* **22**, 9708–9720 (2002).
44. E. Jho *et al.*, Wnt/beta-catenin/Tcf signaling induces the transcription of Axin2, a negative regulator of the signaling pathway. *Mol. Cell. Biol.* **22**, 1172–1183 (2002).
45. L. Varela-Nallar, C. P. Grabowski, I. E. Alfaro, A. R. Alvarez, N. C. Inestrosa, Role of the Wnt receptor Frizzled-1 in presynaptic differentiation and function. *Neural Dev.* **4**, 41 (2009).
46. O. Söderberg *et al.*, Direct observation of individual endogenous protein complexes in situ by proximity ligation. *Nat. Methods*. **3**, 995–1000 (2006).

47. A. Klaesson *et al.*, Improved efficiency of in situ protein analysis by proximity ligation using UnFold probes. *Sci. Rep.* **8**, 5400 (2018).
48. C. Niehrs, J. Shen, Regulation of Lrp6 phosphorylation. *Cell Mol. Life Sci.* **67**, 2551–2562 (2010).
49. T. Saito *et al.*, Single App knock-in mouse models of Alzheimer's disease. *Nat. Neurosci.* **17**, 661–663 (2014).
50. J. B. J. van Meurs *et al.*, Common genetic variation of the low-density lipoprotein receptor-related protein 5 and 6 genes determines fracture risk in elderly white men. *J. Bone Miner. Res.* **21**, 141–150 (2006).
51. R. Sarzani *et al.*, Carotid artery atherosclerosis in hypertensive patients with a functional LDL receptor-related protein 6 gene variant. *Nutr Metab Cardiovasc Dis*. **21**, 150–156 (2011).
52. K. I. Pinson, J. Brennan, S. Monkley, B. J. Avery, W. C. Skarnes, An LDL-receptor-related protein mediates Wnt signalling in mice. *Nature*. **407**, 535–538 (2000).
53. A. M. M. Orellana *et al.*, Age-related neuroinflammation and changes in AKT-GSK-3β and WNT/ β-CATENIN signaling in rat hippocampus. *Aging (Albany, NY)*. **7**, 1094–1111 (2015).
54. J. Folke, B. Pakkenberg, T. Brudek, Impaired wnt signaling in the prefrontal cortex of alzheimer's disease. *Mol. Neurobiol.* **56**, 873–891 (2019).
55. L. Cong *et al.*, Multiplex genome engineering using CRISPR/Cas systems. *Science*. **339**, 819–823 (2013).
56. J.-C. Hsieh *et al.*, Mesd encodes an LRP5/6 chaperone essential for specification of mouse embryonic polarity. *Cell*. **112**, 355–367 (2003).
57. F. McLeod, A. Marzo, M. Podpolny, S. Galli, P. Salinas, Evaluation of synapse density in hippocampal rodent brain slices. *J. Vis. Exp.* (2017), doi:10.3791/56153.
58. E. K. Pickett *et al.*, Amyloid beta and tau cooperate to cause reversible behavioral and transcriptional deficits in a model of alzheimer's disease. *Cell Rep.* **29**, 3592–3604.e5 (2019).
59. B.-K. Koo *et al.*, Tumour suppressor RNF43 is a stem-cell E3 ligase that induces endocytosis of Wnt receptors. *Nature*. **488**, 665–669 (2012).

Acknowledgments

We would like to thank Professors Takashi Saito and Takaomi Saido for the NL-G-F mice, Professor Pico Caroni for the *Thy1-GFP* mice, Professors Xi He, Randall Moon, Bernadette Holdener and Yukiko Goda for DNA constructs and Professor Frances Brodsky for cell lines. We would like to thank Dr Ian White for performing the EM. We would like to thank to members of our lab for insightful discussions on the data and comments on our manuscript. Diagrams were created with BioRender.com.

Funding

MRC MR/M024083/1 (PCS)

MRC MR/S012125/1 (PCS)

ARUK ARUK-PPG2021B/030 (PCS)

Alzheimer's Society AS-PG-17-006 (PCS)

MRC MC_ST_LMCB_2019 (MEJ)

Wellcome Trust 102267/Z/13/Z (JB)

Author contributions

Conceptualization: PCS
Methodology: EM, KB, MEJ, JB, TD, NMF, ST, EP
Investigation: MEJ, JB, TD, NMF, ST, EP
Visualization: MEJ, JB, TD, NMF, ST, EP
Supervision: PCS, AG
Writing—original draft: PCS, MEJ, JB
Writing—review & editing: PCS, MEJ, JB, AG, TD, EM, NMF, ST, EP

Competing interests

The authors declare that they have no competing interests.

Data and materials availability

All data needed to evaluate the conclusions in the paper are present in the main text and/or the supplementary materials.

Figures

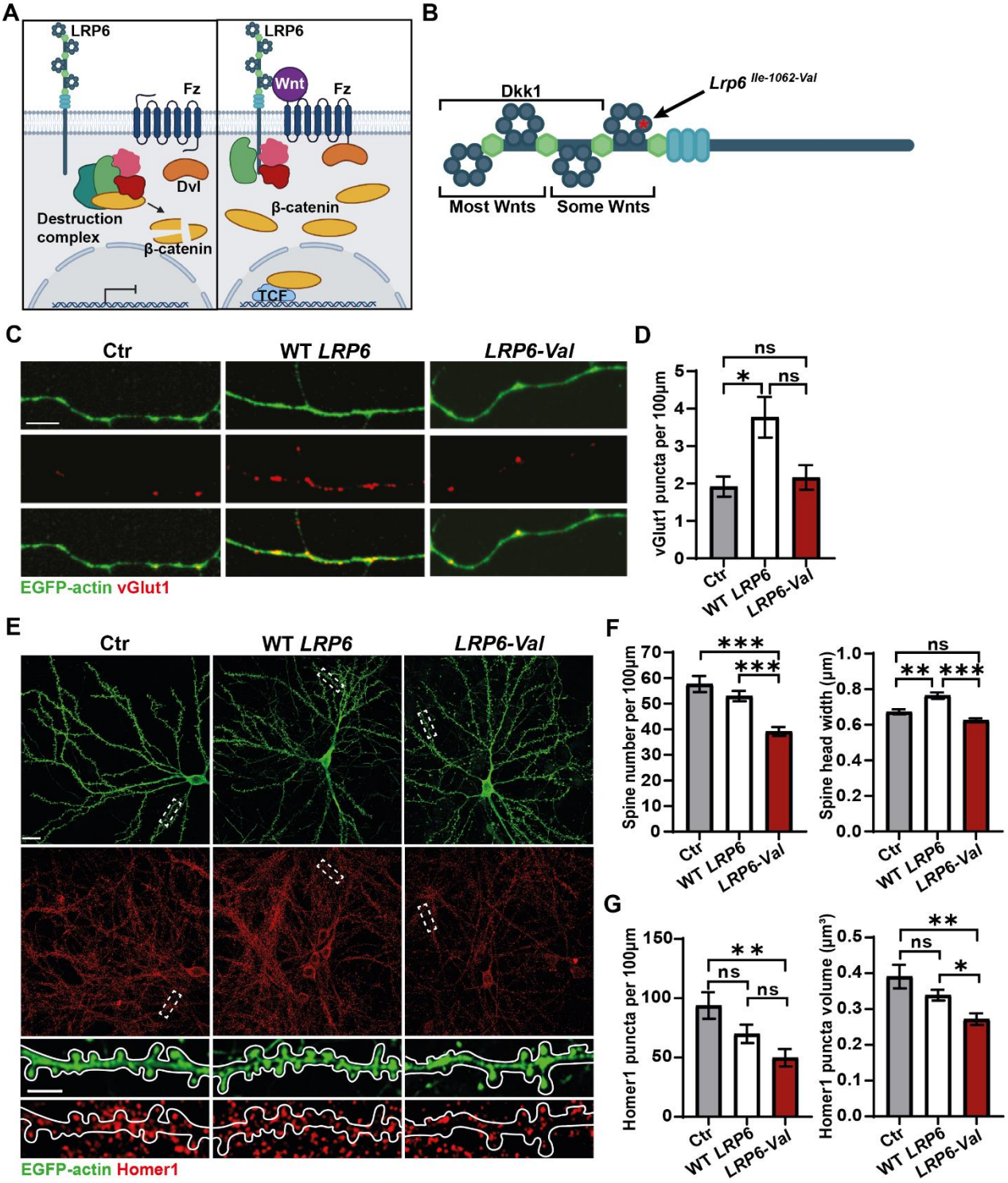

Figure 1

Figure 1. Expression of *LRP6-Val* induces synaptic defects in cultured neurons. A) Diagram of canonical Wnt signalling. Left: in the absence of Wnt, β-catenin is sequestered and degraded by the destruction complex preventing transcription of Wnt target genes. Right: Wnt, LRP6 and Fz receptors form a complex. Activation of the pathway results in Dishevelled (Dvl) recruitment to the plasma membrane and disassembly of the destruction complex. β-catenin accumulates and translocates to the nucleus enabling Wnt target gene transcription. **B**) Schematic of LRP6 showing the location of the *Lrp6-val* SNP (red asterisk and arrow) and the areas to which the Wnt antagonist Dkk1 and Wnt ligands bind. **C**) Confocal images of vGlut1 (red) puncta on isolated axons of neurons expressing EGFP-actin alone or EGFP-actin and human WT *LRP6* or human *LRP6-Val*. Scale bar = 5 μm. **D**) WT *LRP6* promoted the assembly of presynaptic sites but *LRP6-Val* did not. N = 4 independent cultures, 10-12 axons per culture. Kruskal-Wallis with Dunn's post-hoc test. **E**) Top: Confocal images of Homer1 (red) and GFP (green) of neurons expressing EGFP-actin and human WT *LRP6* or human *LRP6-Val*. Scale bar = 21 μm. Bottom: Higher magnification images show dendritic spines (GFP; green) and Homer1 (red) puncta along dendrites. Scale bar = 5 μm. **F**) Left panel: Expression of *LRP6-Val* reduced spine density. 3 independent cultures, 8-10 cells per culture. One-way-ANOVA with Tukey's post-hoc test. Right panel: Expression of *LRP6-Val* failed to increase spine size. N = 3 independent cultures, 8-10 cells per culture. Kruskal-Wallis with Dunn's post-hoc. **G**) *LRP6-Val* expression led to smaller and fewer Homer1 puncta. N = 3 independent cultures, 8-10 images per culture. One-way-ANOVA with Tukey's post-hoc test. Data are represented as mean ± SEM. * $p < 0.05$, ** $p < 0.01$. *** $p < 0.001$.

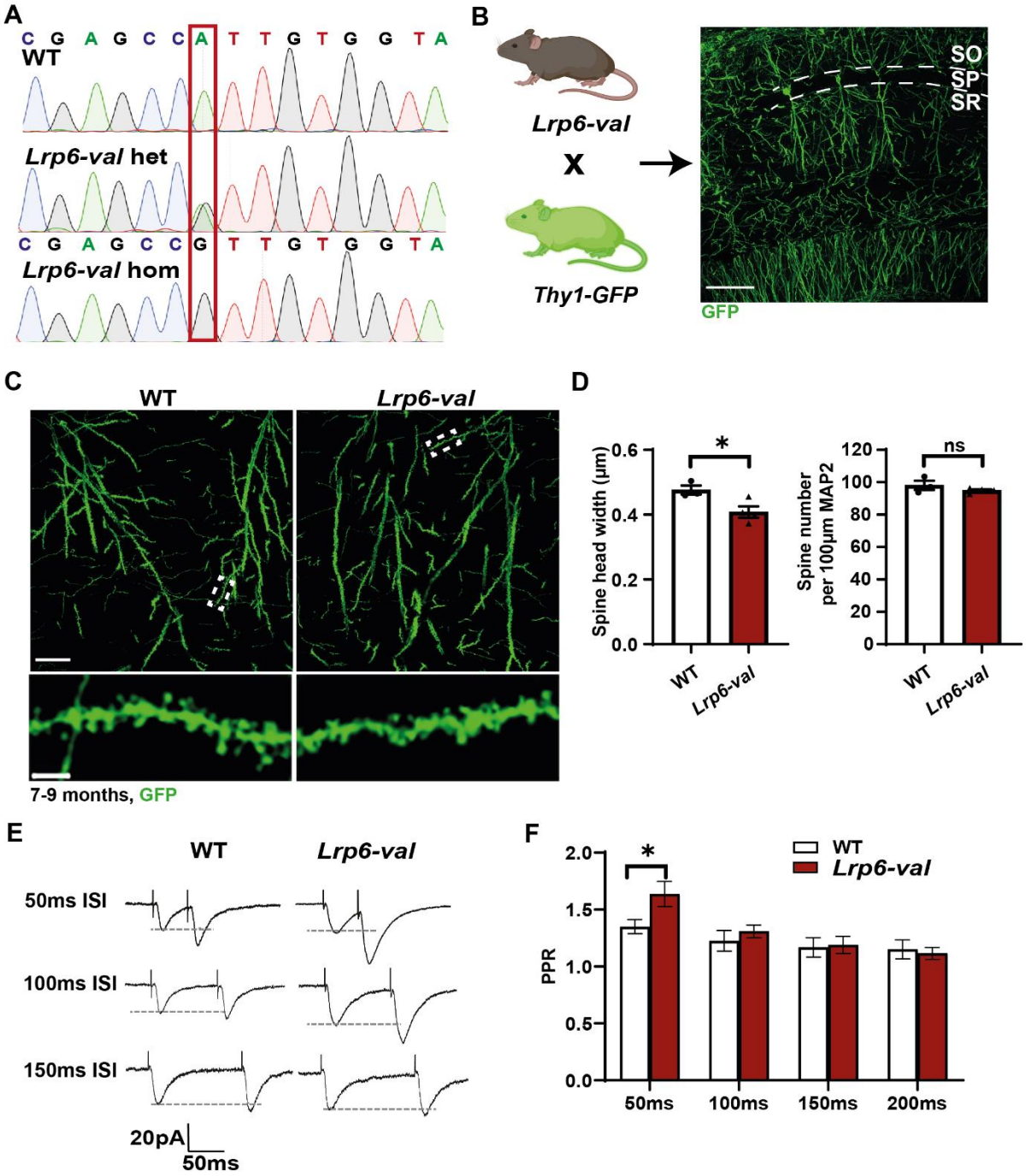
A
C G A G C C A T T G T G G T A
WT
Lrp6-val het
C G A G C C G T T G T G G T A
Lrp6-val hom
B
Lrp6-val
X
Thy1-GFP
SO
SP
SR
GFP
C
WT
Lrp6-val
7-9 months, GFP
D
Spine head width (µm)
0.6
0.4
0.2
0.0
*
WT
Lrp6-val
Spine number per 100µm MAP2
120
100
80
60
40
20
0
ns
WT
Lrp6-val
E
WT
Lrp6-val
50ms ISI
100ms ISI
150ms ISI
20pA
50ms
F
PPR
2.0
1.5
1.0
0.5
0.0
*
WT
Lrp6-val
50ms
100ms
150ms
200ms

Figure 2

Figure 2. *Lrp6-val* mice exhibit synaptic defects at 7-9 months. A) Sanger trace examples of WT, *Lrp6-val* heterozygous (*Lrp6-val* het) and *Lrp6-val* homozygous (*Lrp6-val* hom) knock-in mice. **B**) Dendritic spines were analysed in *Lrp6-val* hom knock-in mice crossed to a *Thy1-GFP* line. SO = stratum oriens, SP = stratum pyramidale, SR = stratum radiatum. Scale bar = 100 µm. **C**) Confocal images of apical dendrites of CA1 pyramidal neurons of WT and *Lrp6-val* mice at 7-9 months. Scale bar = 25 µm. Inset shows spines along a dendrite. Scale bar = 3 µm. **D**) *Lrp6-val* mice display reduced spine head width. WT N = 3 *Lrp6-val* N = 4. Unpaired T-test. * $p < 0.05$. **E**) Representative paired-pulse recordings of synaptic currents from WT and *Lrp6-val* brain slices at different inter-stimulus intervals (ISIs). **F**) Graph displays the mean PPR from all recorded cells. *Lrp6-val* increased the PPR at 50 ms inter-stimulus intervals. N = 11-21 cells recorded from 4-5 animals per genotype. Repeated measures one-way-ANOVA with Tukey's post-hoc test. * $p < 0.05$. Data are represented as mean ± SEM.

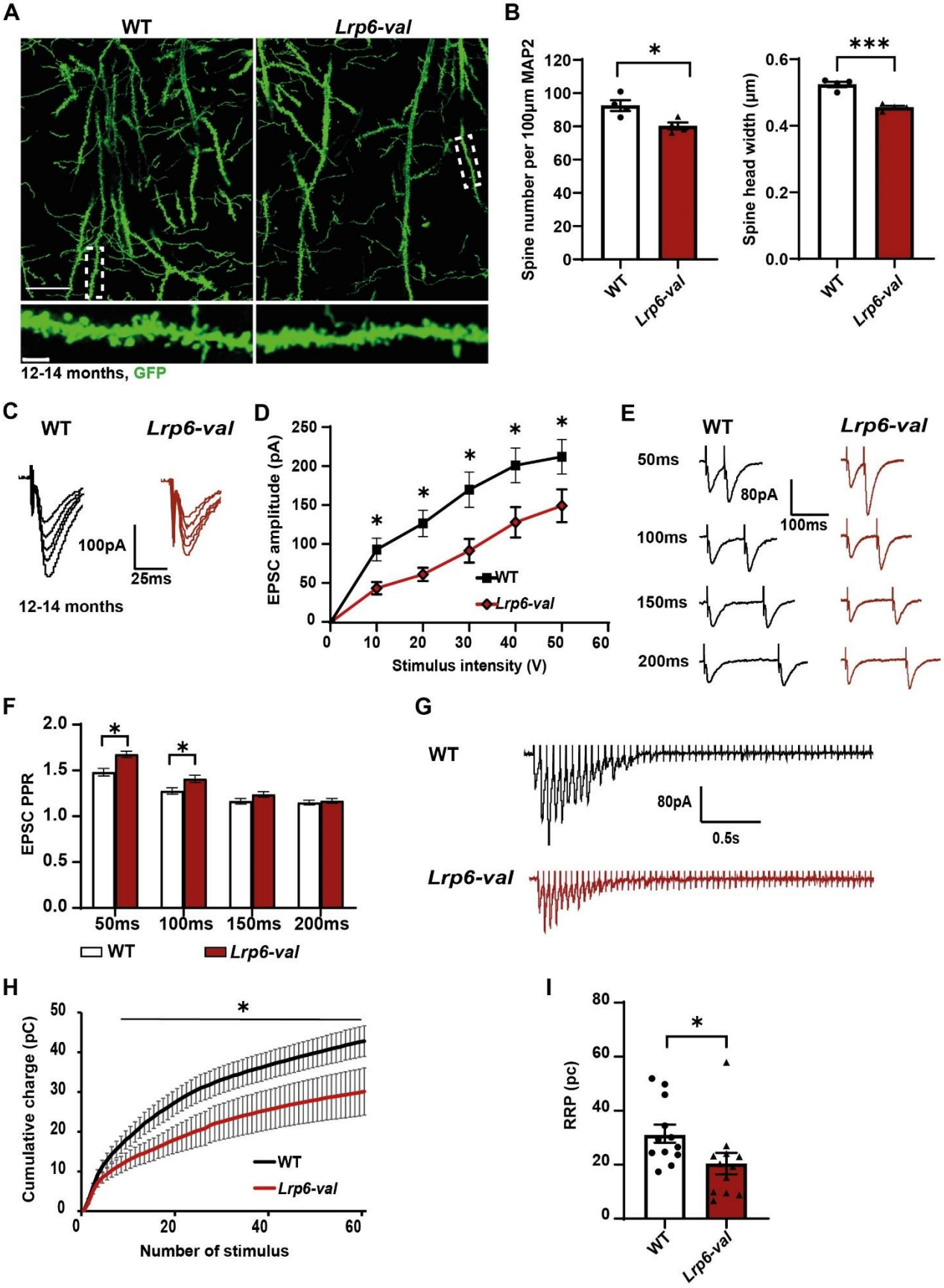
A
WT
Lrp6-val
12-14 months, GFP
B
Spine number per 100μm MAP2
Spine head width (μm)
WT
Lrp6-val
C
WT
Lrp6-val
100pA
25ms
12-14 months
D
EPSC amplitude (pA)
Stimulus intensity (V)
WT
Lrp6-val
E
WT
Lrp6-val
50ms
100ms
150ms
200ms
80pA
100ms
F
EPSC PPR
50ms
100ms
150ms
200ms
WT
Lrp6-val
G
WT
Lrp6-val
80pA
0.5s
H
Cumulative charge (pC)
Number of stimulus
WT
Lrp6-val
I
RRP (pc)
WT
Lrp6-val

Figure 3

Figure 3. *Lrp6-val* mice display postsynaptic defects and impaired basal synaptic transmission, synaptic vesicle release and RRP size at 12 months. A) Top: Dendritic spines were analysed at 12-14 months in *Lrp6-val* knock-in mice crossed to a *Thy1-GFP* line. Scale bar = 25 µm. Bottom: Confocal images of regions of interest containing apical dendrites of CA1 pyramidal neurons in WT and *Lrp6-val* mice. Scale bar = 3 µm. **B**) *Lrp6-val* mice have smaller and fewer spines. WT N = 4, *Lrp6-val* N = 4. Unpaired T-test. **C**) Representative traces of evoked excitatory post-synaptic currents (EPSCs) elicited at increasing stimulation voltages with an average of three responses for each stimulus voltage. **D**) Input-output curves showing a significant reduction in EPSC amplitude in hippocampal slices from *Lrp6-val* mice. N = 12-13 cells from 4 animals per genotype. Repeated measure one-way-ANOVA with Tukey's post-hoc test. **E**) Representative traces of paired pulse evoked EPSCs at different interstimulus intervals using brain slices from WT and *Lrp6-val* mice. **F**) Graph displays the mean PPR from all cells. *Lrp6-val* mice display increased PPR at 50 ms and 100 ms ISI. *N* = 13-14 cells from 4 animals per genotype. Repeated measure one-way-ANOVA with Tukey's post-hoc test. **G**) Representative traces of EPSCs elicited by a 20 Hz electrical stimulation for 3 s recorded from WT and *Lrp6-val* mice. **H**) Graph showing reduced mean cumulative charge in *Lrp6-val* mice. *N* = 12 cells from 4 animals per genotype. Repeated measure one-way-ANOVA with Tukey's post-hoc test. **I**) Graph displays the readily releasable pool (RRP) size, obtained from all cells. *Lrp6-val* mice exhibited a reduced RRP. *N* = 12 cells from 4 animals per genotype. Unpaired Student's *T-t*est. Data are represented as mean ± SEM. * $p < 0.05$, *** $p < 0.001$.

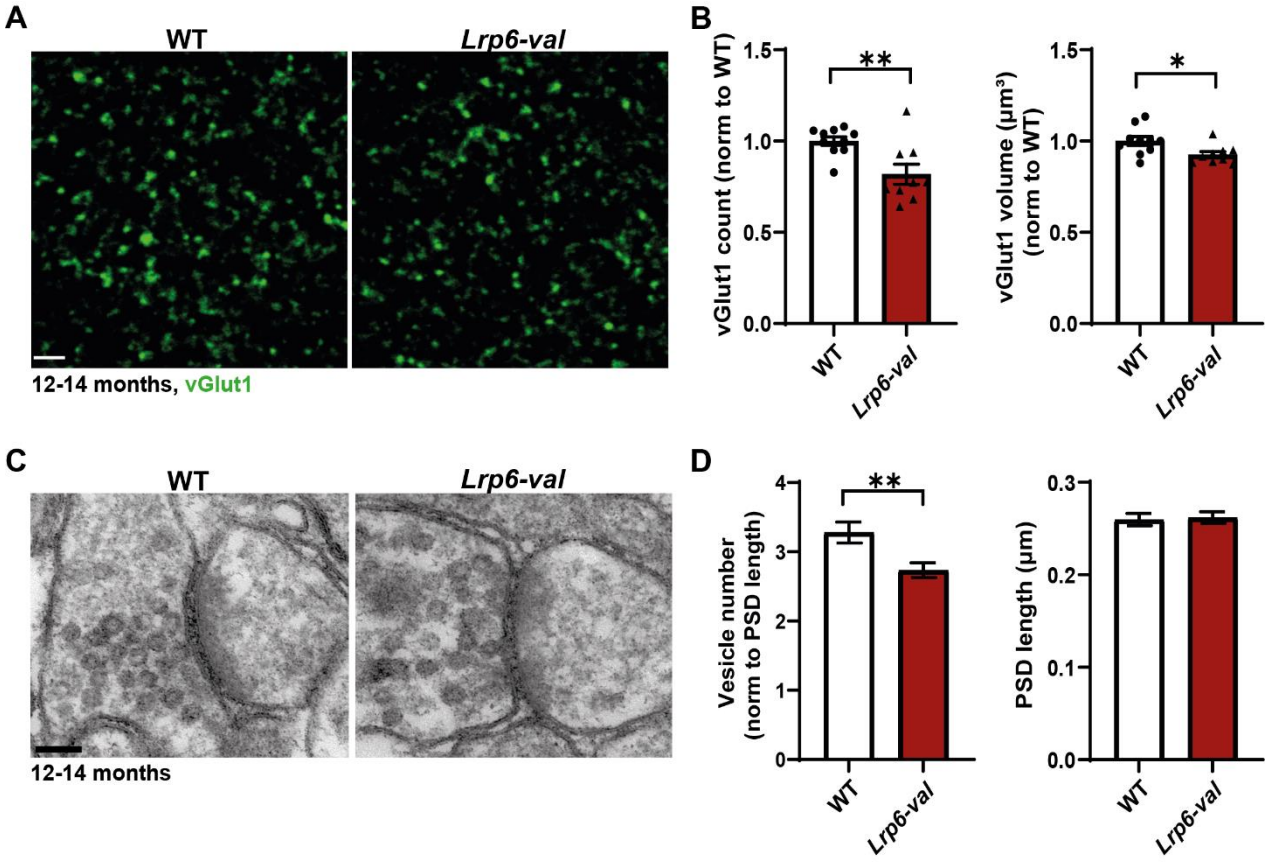
A
WT
Lrp6-val
12-14 months, vGlut1
B
vGlut1 count (norm to WT)
1.5
1.0
0.5
0.0
**
WT
Lrp6-val
vGlut1 volume (µm³) (norm to WT)
1.5
1.0
0.5
0.0
*
WT
Lrp6-val
C
WT
Lrp6-val
12-14 months
D
Vesicle number (norm to PSD length)
4
3
2
1
0
**
WT
Lrp6-val
PSD length (µm)
0.3
0.2
0.1
0.0
WT
Lrp6-val

Figure 4

Figure 4. Presynaptic defects of *Lrp6-val* mice at 12-14 months. A) Confocal images of vGlut1-labelled excitatory presynaptic terminals in the CA1 stratum radiatum area of WT and *Lrp6-val* mice at 12-14 months. Scale bar = 2 µm. **B**) *Lrp6-val* mice had fewer and smaller vGlut1 puncta. WT N = 10 *Lrp6-val* N = 9. Unpaired T-test. * $p < 0.05$, ** $p < 0.01$. **C**) Electron microscopy images of an excitatory synapse of 12-14-month-old WT and *Lrp6-val* mice. Scale bar = 100 nm. **D**) *Lrp6-val* mice had fewer synaptic vesicles but no changes in PSD length were observed. N = 5, 19-25 images per animal. Mann-Whitney test. ** $p < 0.01$. Data are represented as mean ± SEM.

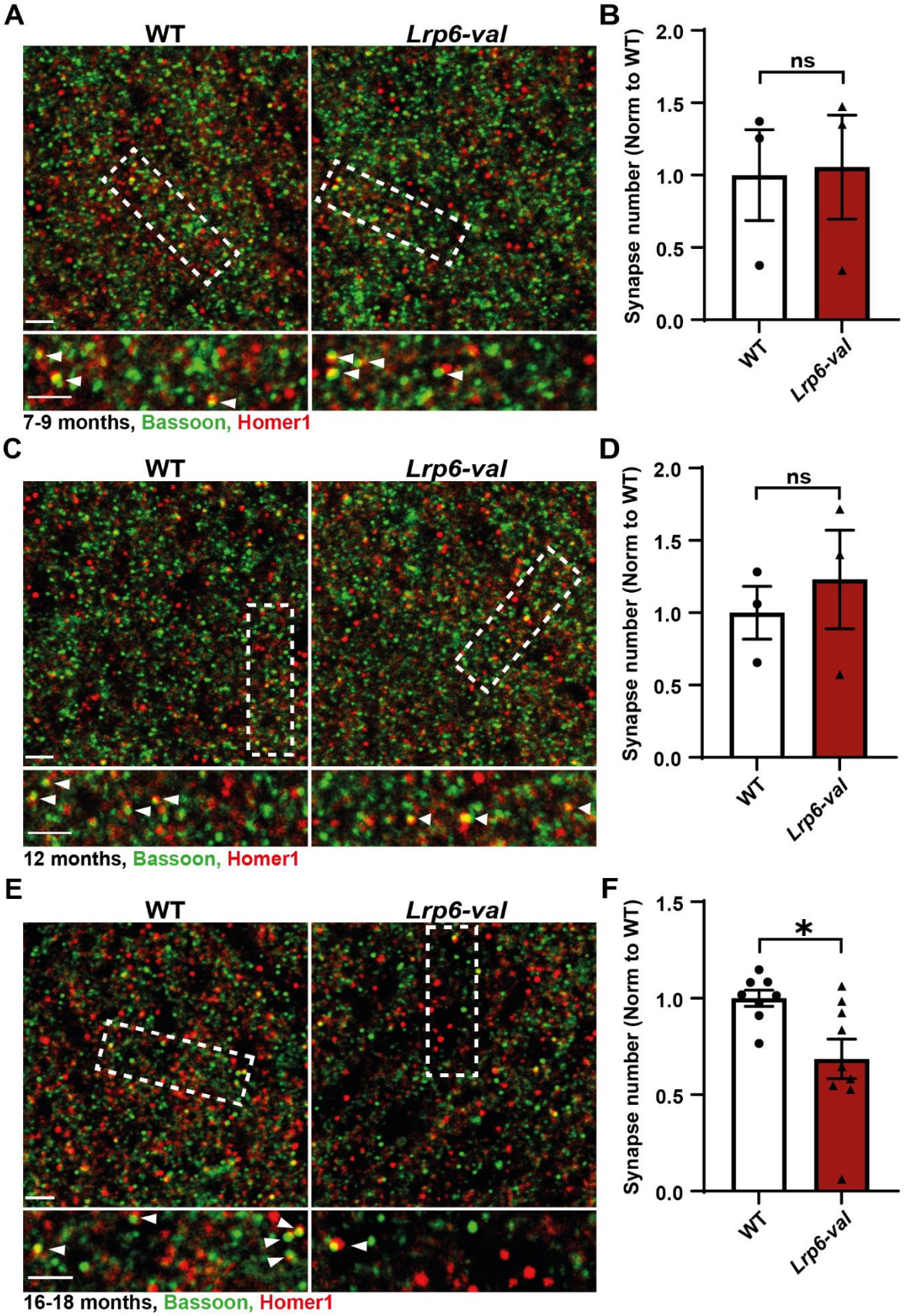
A
WT
Lrp6-val
7-9 months, Bassoon, Homer1
B
Synapse number (Norm to WT)
2.0
1.5
1.0
0.5
0.0
ns
WT
Lrp6-val
C
WT
Lrp6-val
12 months, Bassoon, Homer1
D
Synapse number (Norm to WT)
2.0
1.5
1.0
0.5
0.0
ns
WT
Lrp6-val
E
WT
Lrp6-val
16-18 months, Bassoon, Homer1
F
Synapse number (Norm to WT)
1.5
1.0
0.5
0.0
*
WT
Lrp6-val

Figure 5

Figure 5. *Lrp6-val* mice exhibit synapse loss with age. A, **C**, **E**) Confocal images of the CA1 stratum radiatum of WT and *Lrp6-val* mice labelled with Bassoon (green) and Homer1 (red) at 7-9 months (**A**), 12 months (**C**) and 16-18 months (**E**). Scale bar = 2.5 µm. Insets display high magnification images of synapses. Scale bar = 2 µm. **B** and **D**) Quantification of synapse number, based on the co-localisation of pre- and post-synaptic puncta, showed no differences between WT and *Lrp6-val* mice at 7-9 months (**B**) or 12 months (**D**). N = 3 per genotype. Unpaired T-test. **F**) Synapse number was significantly reduced in *Lrp6-val* mice 16-18 months. WT N = 8, *Lrp6-val* N = 9. Unpaired T-test. * $p < 0.05$. Data are represented as mean ± SEM.

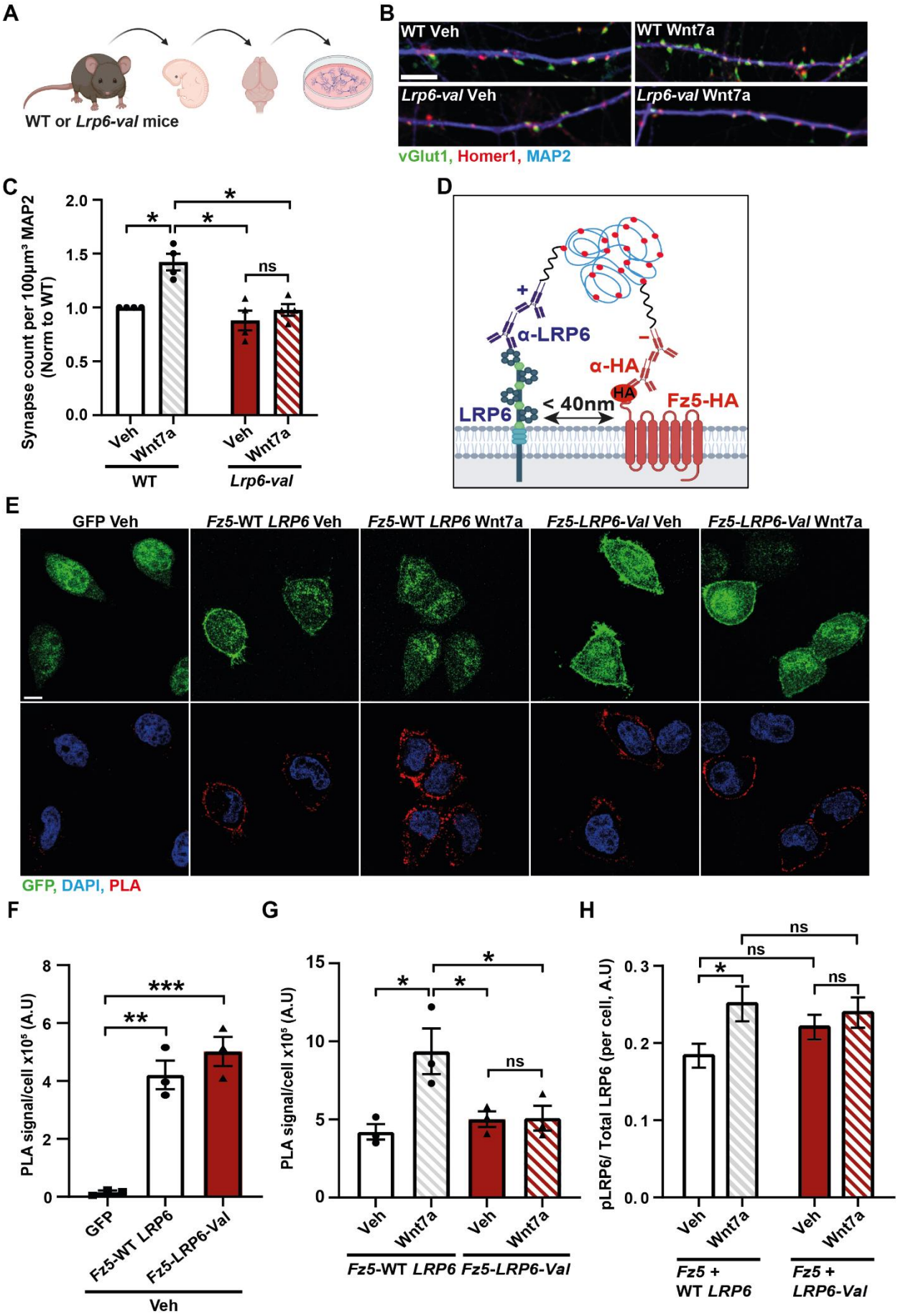
A
WT or Lrp6-val mice
B
WT Veh
WT Wnt7a
Lrp6-val Veh
Lrp6-val Wnt7a
vGlut1, Homer1, MAP2
C
Synapse count per 100µm³ MAP2 (Norm to WT)
2.0
1.5
1.0
0.5
0.0
*
*
*
ns
Veh
Wnt7a
Veh
Wnt7a
WT
Lrp6-val
D
α-LRP6
α-HA
HA
< 40nm
LRP6
Fz5-HA
E
GFP Veh
Fz5-WT LRP6 Veh
Fz5-WT LRP6 Wnt7a
Fz5-LRP6-Val Veh
Fz5-LRP6-Val Wnt7a
GFP, DAPI, PLA
F
PLA signal/cell x10⁵ (A.U)
8
6
4
2
0
***
**
GFP
Fz5-WT LRP6
Fz5-LRP6-Val
Veh
G
PLA signal/cell x10⁵ (A.U)
15
10
5
0
*
*
*
ns
Veh
Wnt7a
Veh
Wnt7a
Fz5-WT LRP6
Fz5-LRP6-Val
H
pLRP6/ Total LRP6 (per cell, A.U)
0.3
0.2
0.1
0.0
ns
ns
*
ns
Veh
Wnt7a
Veh
Wnt7a
Fz5 + WT LRP6
Fz5 + LRP6-Val

Figure 6

Figure 6. Neurons from *Lrp6-val* mice fail to respond to Wnt7a and the presence of *LRP6-Val* affects the Wnt receptor complex and Wnt signalling. A) Diagram depicting hippocampal neuron isolation from WT and *Lrp6-val* mice. **B**) Images of WT and *Lrp6-val* neurons treated with Wnt7a. vGlut1 (green), Homer1 (red) and MAP2 (Blue). Scale bar = 5 µm. **C**) Wnt7a (200ng/ml) increased synapse number in WT neurons, but not in *Lrp6-val* neurons. N = 4 independent cultures. Two-way-ANOVA with Games-Howell post hoc test. **D**) Schematic of PLA to detect LRP6 and Fz5-HA interaction in close proximity (<40 nm). **E**) Confocal images of HeLa cells expressing GFP (control), *Fz5-HA* and WT *LRP6* or *LRP6-Val* treated with control vehicle or Wnt7a. GFP (green), PLA (red) and DAPI (Blue). Scale bar = 10 µm. **F**) The PLA signal intensity per cell was increased in cells expressing *Fz5-HA* and WT *LRP6* or *LRP6-Val* compared to cells expressing GFP. N = 3 independent experiments. One-way-ANOVA with Tukey's post-hoc test. **G**) Wnt7a increased the PLA signal in cells expressing WT *LRP6* and *Fz5-HA* but not in cells expressing *LRP6-Val* and *Fz5-HA*. N = 3 independent experiments. Two-way-ANOVA with Tukey's post hoc test. **H**) Wnt7a increased the ratio of phosphorylated LRP6 (pLRP6) to total LRP6 in HeLa cells expressing WT *LRP6* and *Fz5-HA* but not in cells expressing *LRP6-Val* and *Fz5-HA*. WT *LRP6* + *Fz5-HA* Veh N = 50 cells, WT *LRP6* + *Fz5-HA* Wnt7a N = 53 cells, *LRP6-Val* + *Fz5-HA* Veh N = 71 cells, *LRP6-Val* + *Fz5-HA* Wnt7a N = 61 cells, from 3 independent experiments. Kruskal-Wallis with Dunn's post-hoc test. Data are represented as mean ± SEM. * $p < 0.05$, ** $p < 0.01$ and *** $p < 0.001$.

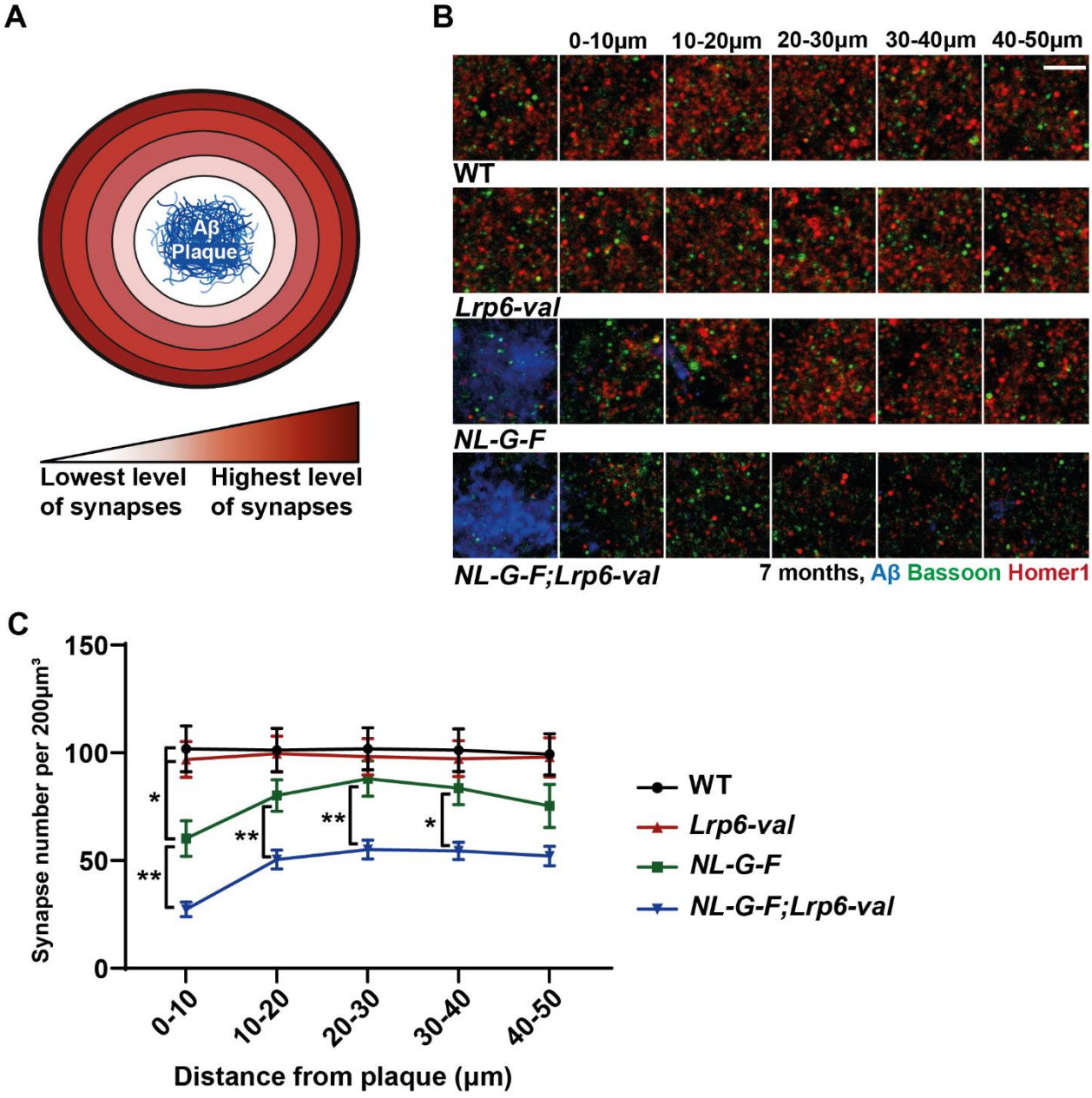
A
Aβ
Plaque
Lowest level of synapses
Highest level of synapses
B
0-10μm
10-20μm
20-30μm
30-40μm
40-50μm
WT
Lrp6-val
NL-G-F
NL-G-F;Lrp6-val
7 months, Aβ Bassoon Homer1
C
Synapse number per 200μm³
150
100
50
0
0-10
10-20
20-30
30-40
40-50
Distance from plaque (μm)
WT
Lrp6-val
NL-G-F
NL-G-F;Lrp6-val

Figure 7

Figure 7. *Lrp6-val* exacerbates synapse loss around plaques in NL-G-F mice at 7 months. A) Diagram shows synapse loss around an Aβ plaque (blue). **B**) Confocal images of Bassoon (green) and Homer1 (red) at increasing distances from the centre of an Aβ plaque (blue) in *NL-G-F* and *NL-G-F;Lrp6-val* mice, or an equivalent point in WT and *Lrp6-val* mice, in the CA1 stratum radiatum at 7 months. Scale bar = 4 µm. **C**) *NL-G-F* mice displayed fewer synapses compared to WT mice or to *Lrp6-val* mice at 0-10 µm from the centre of a plaque. Synapse number was reduced in *NL-G-F;Lrp6-val* at 0-40 µm from the center of a plaque compared to *NL-G-F* mice. A significant reduction in synapse number was detected in *NL-G-F;Lrp6-val* when compared to WT mice or *Lrp6-val* mice at all distances from the center of a plaque. WT = 17 slices from 6 animals, *Lrp6-val* = 18 slices from 6 animals, *NL-G-F* = 18 slices from 7 animals, *NL-G-F;Lrp6-val* = 19 slices from 7 animals. Repeated measure Two-way-ANOVA with Tukey's post hoc test. * $p < 0.05$, ** $p < 0.01$. Data are represented as mean ± SEM.